

Analysis of T_{cc} and T_{bb} based on the hadronic molecular model and their spin multiplets

Manato Sakai^{✉*}

Department of Physics, Nagoya University, Nagoya 464-8602, Japan

Yasuhiro Yamaguchi^{✉†}

*Department of Physics, Nagoya University, Nagoya 464-8602, Japan;
Kobayashi-Maskawa Institute for the Origin of Particles and the Universe,
Nagoya University, Nagoya, 464-8602, Japan
and Meson Science Laboratory, Cluster for Pioneering Research,
RIKEN, Hirosawa, Wako, Saitama 351-0198, Japan*

 (Received 20 December 2023; accepted 8 February 2024; published 11 March 2024)

$T_{cc}(cc\bar{u}\bar{d})^+$ has been reported by the LHCb experiment in 2022. The analysis using the Breit-Wigner parametrization found the small binding energy, 0.273 MeV, which is measured from the threshold of $D^{*+}D^0$. In this paper, we consider T_{cc} as a DD^* hadronic molecule as a deuteronlike state. The one-boson exchange model is employed as for the heavy meson interactions, where we determine the cutoff parameter Λ to reproduce the reported binding energy of T_{cc} with $I(J^P) = 0(1^+)$. We discuss the properties of the bound state and also search for T_{cc} with quantum numbers other than $0(1^+)$. Furthermore, we analyze T_{bb} as a bottom counterpart of T_{cc} , which involves two bottom quarks, and obtain several bound states. Finally, we consider the light-cloud basis for wave functions of the doubly heavy tetraquarks in the heavy quark limit. Using the basis, we find the spin multiplets of their bound states, indicating the spin structures of diquarks in T_{cc} and T_{bb} with the finite quark masses.

DOI: [10.1103/PhysRevD.109.054016](https://doi.org/10.1103/PhysRevD.109.054016)

I. INTRODUCTION

Most hadrons can be classified into baryons consisting of three quarks qqq and mesons consisting of a quark and an antiquark $q\bar{q}$. However, hadrons with more than three quarks are not prohibited in quantum chromodynamics (QCD), which was already indicated by Gell-Mann and Zweig [1–3]. Hadrons like these states which cannot be explained by ordinary hadrons $q\bar{q}$ and qqq are called exotic hadrons. In the heavy quark sector, various exotic hadrons such as X , Y , Z , and P_c have been reported since the report on $X(3872)$ in 2003 [4–10]. The structures and interactions of these states are not well understood, and these studies are important subjects of current research in hadron physics.

In 2022, $T_{cc}(cc\bar{u}\bar{d})^+$ has been reported by the LHCb experiment. The Breit-Wigner mass relative to the $D^{*+}D^0$ mass threshold δm_{BW} is

$$\delta m_{\text{BW}} = -273 \pm 61 \pm 5_{-14}^{+11} \text{ keV}/c^2,$$

while the pole mass relative to the $D^{*+}D^0$ mass threshold δm_{pole} is

$$\delta m_{\text{pole}} = -360 \pm 40_{-0}^{+4} \text{ keV}/c^2,$$

respectively [9,11]. The charm number is 2 and the baryon number is 0; thus, this state is considered as a genuine exotic state. The isospin, spin, and parity are considered as $I(J^P) = 0(1^+)$. T_{cc} has widely been studied before the report on $T_{cc}(cc\bar{u}\bar{d})^+$ by the LHCb experiment. In the 1980s, there were theoretical studies by using the non-relativistic quark model [12–14]. Many theoretical studies also have been conducted by using many models such as the hadronic molecule [15–22], various quark models [23–25], heavy quark symmetry [26,27], the string model [28], QCD sum rules [29–33], lattice QCD [34–36], and so on as summarized in recent reviews [10].

The small binding energy of T_{cc} from the DD^* threshold motivates us to study the DD^* molecular structure. When considering a hadronic molecule with heavy quarks, we respect the heavy quark spin symmetry (HQS) [37–39]. The HQS leads to mass degeneracy of the heavy pseudo-scalar and vector mesons because of suppression of the

*msakai@hken.phys.nagoya-u.ac.jp

†yamaguchi@hken.phys.nagoya-u.ac.jp

Published by the American Physical Society under the terms of the Creative Commons Attribution 4.0 International license. Further distribution of this work must maintain attribution to the author(s) and the published article's title, journal citation, and DOI. Funded by SCOAP³.

chromomagnetic interaction in the heavy quark limit. In fact, the mass difference of D and D^* is approximately 140 MeV, which is smaller than those in the light quark sectors, e.g., $m_\rho - m_\pi \sim 630$ MeV and $m_{K^*} - m_K \sim 390$ MeV. Thus, D and D^* are considered as the HQS doublet. B and B^* are considered in the same way, because the mass difference of B and B^* is approximately 45 MeV. Thus, in a hadronic molecular system of two mesons, these facts lead to channel coupling of PP , PP^* , and P^*P^* ($P = D, B$ and $P^* = D^*, B^*$).

The HQS multiplets can be also seen in a hadronic molecule by using the light-cloud basis (LCB) [40–42]. The light-cloud basis can be obtained by a unitary transformation of the hadronic-molecule basis (HMB), where the spin wave function of the hadronic molecule is decomposed into spins of heavy quarks and the light cloud. Thus, we can see the spin structures of quarks in the LCB, which are hidden in the HMB, and the states can be classified by the quark spin structures. The HQS multiplet of the hadronic molecule with a single heavy quark has been discussed in Ref. [40]. In Ref. [42], the author has classified the hidden-charm pentaquark P_c by using the LCB. Interestingly, the HQS multiplets indicate the existence of partners. Since states with the same spin structures of diquarks belong to the same HQS multiplets, the existence of one state indicates that of partners.

In this paper, we study the doubly heavy tetraquarks T_{cc} and the bottom counterpart T_{bb} as a hadronic molecule of two mesons. In Ref. [16], the author has studied the doubly heavy tetraquarks with several quantum numbers as the hadronic molecules of $D^{(*)}D^{(*)}$ and $B^{(*)}B^{(*)}$ before the LHCb observation. This study has used the one-pion exchange potential (OPEP) and the one-boson exchange potential (OBEP), with the addition of ρ and ω . We follow the study in Ref. [16], and, in addition, we also consider the one- σ meson exchange in the OBEP to construct a more realistic interaction. We determine the cutoff parameter Λ for the OBEP to reproduce the empirical binding energy of T_{cc} with $I(J^P) = 0(1^+)$. We also study the properties of the obtained bound state. T_{cc} with quantum numbers other than $0(1^+)$ is also investigated. Using the same potentials, we discuss the existence of T_{bb} as the $B^{(*)}B^{(*)}$ molecule. Finally, we apply the LCB to the doubly heavy tetraquarks in the heavy quark limit, where the bound states are classified by their spin structures of heavy diquark and light antidiquark. The obtained HQS multiplet structure indicates the existence of partner states of the tetraquark bound states.

This paper is organized as follows. In Sec. II, we introduce the formalisms of the OPEP and the OBEP. In Sec. III, we show our numerical results for the bound states of T_{cc} and T_{bb} with given $I(J^P)$ and discuss the spin structures of the bound states obtained by our analyses. In Sec. IV, we summarize our results and discussions.

II. FORMALISM

A. Lagrangian

In the heavy quark limit (HQL), the heavy pseudoscalar and heavy vector mesons which include the heavy quarks are degenerate due to HQS. Therefore, we define the heavy meson field H_a written as the direct sum of the heavy pseudoscalar meson field P_a and the heavy vector meson field $P_{a\mu}$ as follows [37–39]:

$$H_a = \frac{1 + \not{v}}{2} [P_{a\mu}^* \gamma^\mu - P_a \gamma_5], \quad (1)$$

$$\bar{H}_a = \gamma_0 H_a^\dagger \gamma_0 = [P_{a\mu}^{*\dagger} \gamma^\mu + P_a^\dagger \gamma_5] \frac{1 + \not{v}}{2}. \quad (2)$$

\bar{H}_a is the complex conjugate of H_a . Here, v^μ is the four-velocity of the heavy quark which satisfies $v^2 = 1$, $v^0 > 0$ and $(1 + \not{v})/2$ is the projective operator which projects out the positive-energy component in the heavy quark. Also, the heavy meson field H_a is transformed as $H_a \rightarrow D(\Lambda) H_a D^{-1}(\Lambda)$ under the Lorentz transformation and $H_a \rightarrow S_Q H_a U_q^\dagger$ under the spin transformation for the heavy quark and the chiral transformation for a light quark. Here, $D(\Lambda)$ is the Lorentz transformation matrix, S_Q is the spin transformation matrix, and U_q is the chiral transformation matrix. We construct the interaction effective Lagrangian for a pseudoscalar meson [39]:

$$\mathcal{L}_\pi = ig \text{Tr} [H_b \gamma_\mu \gamma_5 \mathcal{A}_{ba}^\mu \bar{H}_a]. \quad (3)$$

Here, \mathcal{A}^μ is the axial-vector current which is defined by

$$\mathcal{A}_\mu = \frac{1}{2} [\xi^\dagger (\partial_\mu \xi) - \xi (\partial_\mu \xi^\dagger)], \quad (4)$$

where ξ is the nonlinear representation written as

$$\xi = \exp\left(\frac{\vec{\tau} \cdot \vec{\pi}}{2f_\pi}\right) \quad (5)$$

with the pion decay constant $f_\pi \simeq 93$ MeV. The pion field $\hat{\pi}$ is defined by

$$\hat{\pi} = \frac{1}{\sqrt{2}} \begin{pmatrix} \pi^0 & \sqrt{2}\pi^+ \\ \sqrt{2}\pi^- & -\pi^0 \end{pmatrix} = \frac{1}{\sqrt{2}} \vec{\pi} \cdot \vec{\tau}, \quad (6)$$

where $\vec{\tau}$ is the Pauli matrices. We obtain the interaction effective Lagrangians for the $\pi P^{(*)} P^{(*)}$ vertices by expanding Eq. (3) [16]:

$$\mathcal{L}_{\pi P P^*} = -\frac{g}{f_\pi} (P_a^{*\dagger \mu} P_b + P_a^\dagger P_b^{*\mu}) \partial_\mu (\vec{\pi} \cdot \vec{\tau})_{ba}, \quad (7)$$

$$\mathcal{L}_{\pi P^* P^*} = i \frac{g}{f_\pi} \epsilon^{\mu\nu\alpha\beta} v_\mu P_{a\nu}^{*\dagger} P_{b\alpha}^* \partial_\beta (\vec{\pi} \cdot \vec{\tau})_{ba}. \quad (8)$$

However, $\mathcal{L}_{\pi PP} = 0$ due to the parity conservation.

We can also obtain the interaction effective Lagrangians for vector mesons v and a σ meson [39,43]:

$$\mathcal{L}_v = -i\beta \text{Tr}[H_b v^\mu \rho_\mu \bar{H}_a] + i\lambda \text{Tr}[H_b \sigma^{\mu\nu} F_{\mu\nu}(\rho)_{ba} \bar{H}_a], \quad (9)$$

$$\mathcal{L}_\sigma = g_s \text{Tr}[H \sigma \bar{H}], \quad (10)$$

where

$$F_{\mu\nu}(\rho) = \partial_\mu \rho_\nu - \partial_\nu \rho_\mu + [\rho_\mu, \rho_\nu], \quad (11)$$

$$g_V = \frac{m_\rho}{\sqrt{2}f_\pi}, \quad \rho_\mu = \frac{ig_V}{\sqrt{2}} \hat{\rho}_\mu. \quad (12)$$

The vector meson fields $\hat{\rho}_\mu$ are defined by

$$\begin{aligned} \hat{\rho}_\mu &= \frac{1}{\sqrt{2}} \begin{pmatrix} \rho^0 + \omega & \sqrt{2}\rho^+ \\ \sqrt{2}\rho^- & -\rho^0 + \omega \end{pmatrix}_\mu \\ &= \frac{1}{\sqrt{2}} (\vec{\tau} \cdot \vec{\rho}_\mu + \omega \mathbf{1}). \end{aligned} \quad (13)$$

We calculate the Lagrangian for $vP^{(*)}P^{(*)}$ and $\sigma P^{(*)}P^{(*)}$ vertices [16]:

$$\mathcal{L}_v = \mathcal{L}_{vPP} + \mathcal{L}_{vPP^*} + \mathcal{L}_{vP^*P^*}, \quad (14)$$

$$\mathcal{L}_\sigma = \mathcal{L}_{\sigma PP} + \mathcal{L}_{\sigma P^*P^*}, \quad (15)$$

where

$$\mathcal{L}_{vPP} = \sqrt{2}\beta g_V P_b P_a^\dagger v \cdot (\hat{\rho})_{ba}, \quad (16)$$

$$\mathcal{L}_{vPP^*} = -2\sqrt{2}\lambda g_V \epsilon^{\mu\nu\alpha\beta} v_\mu (P_{a\nu}^{*\dagger} P_b + P_a^\dagger P_{\nu b}^*) \partial_\alpha (\hat{\rho})_{ba}, \quad (17)$$

$$\begin{aligned} \mathcal{L}_{vP^*P^*} &= \sqrt{2}\beta g_V P_b^* P_a^{*\dagger} \cdot (\hat{\rho})_{ba} \\ &+ i2\sqrt{2}\lambda g_V P_a^{*\dagger} P_b^{*\nu} (\partial_\mu (\hat{\rho})_{ba} - \partial_\nu (\hat{\rho})_{ba}), \end{aligned} \quad (18)$$

$$\mathcal{L}_{\sigma PP} = -2g_s P^\dagger P \sigma, \quad (19)$$

$$\mathcal{L}_{\sigma P^*P^*} = 2g_s P_\mu^{*\dagger} P^{*\mu} \sigma. \quad (20)$$

B. Hamiltonian

The OBEP is obtained by using these Lagrangians [16].

(i) π :

$$\begin{aligned} V_{PP^*-P^*P}^\pi &= \frac{1}{3} \left(\frac{g}{2f_\pi} \right)^2 [-\vec{\epsilon}^* \cdot \vec{\epsilon} D(r; m_\pi) \\ &+ \vec{\epsilon}^* \cdot \vec{\epsilon} C(r; m_\pi) + S_{\epsilon^* \epsilon} T(r; m_\pi)] \vec{\tau}_1 \cdot \vec{\tau}_2, \end{aligned} \quad (21)$$

$$\begin{aligned} V_{PP^*-P^*P^*}^\pi &= -\frac{1}{3} \left(\frac{g}{2f_\pi} \right)^2 [-\vec{\epsilon}^* \cdot \vec{T} D(r; m_\pi) \\ &+ \vec{\epsilon}^* \cdot \vec{T} C(r; m_\pi) + S_{\epsilon^* T} T(r; m_\pi)] \vec{\tau}_1 \cdot \vec{\tau}_2, \end{aligned} \quad (22)$$

$$\begin{aligned} V_{PP-P^*P^*}^\pi &= \frac{1}{3} \left(\frac{g}{2f_\pi} \right)^2 [-\vec{\epsilon}^* \cdot \vec{\epsilon}^* D(r; m_\pi) \\ &+ \vec{\epsilon}^* \cdot \vec{\epsilon}^* C(r; m_\pi) + S_{\epsilon^* \epsilon^*} T(r; m_\pi)] \vec{\tau}_1 \cdot \vec{\tau}_2, \end{aligned} \quad (23)$$

$$\begin{aligned} V_{P^*P^*-P^*P^*}^\pi &= \frac{1}{3} \left(\frac{g}{2f_\pi} \right)^2 [-\vec{T} \cdot \vec{T} D(r; m_\pi) \\ &+ \vec{T} \cdot \vec{T} C(r; m_\pi) + S_{TT} T(r; m_\pi)] \vec{\tau}_1 \cdot \vec{\tau}_2; \end{aligned} \quad (24)$$

(ii) vector mesons (ρ, ω):

$$V_{PP-PP}^v = \left(\frac{\beta g_V}{2m_v} \right)^2 C(r; m_v) \vec{\tau}_1 \cdot \vec{\tau}_2, \quad (25)$$

$$V_{PP^*-PP^*}^v = \left(\frac{\beta g_V}{2m_v} \right)^2 C(r; m_v) \vec{\tau}_1 \cdot \vec{\tau}_2, \quad (26)$$

$$\begin{aligned} V_{PP^*-P^*P}^v &= \frac{1}{3} (\lambda g_V)^2 [-2\vec{\epsilon}^* \cdot \vec{\epsilon} D(r; m_v) \\ &+ 2\vec{\epsilon}^* \cdot \vec{\epsilon} C(r; m_v) - S_{\epsilon^* \epsilon} T(r; m_v)] \vec{\tau}_1 \cdot \vec{\tau}_2, \end{aligned} \quad (27)$$

$$\begin{aligned} V_{PP^*-P^*P^*}^v &= -\frac{1}{3} (\lambda g_V)^2 [-2\vec{\epsilon}^* \cdot \vec{T} D(r; m_v) \\ &+ 2\vec{\epsilon}^* \cdot \vec{T} C(r; m_v) - S_{\epsilon^* T} T(r; m_v)] \vec{\tau}_1 \cdot \vec{\tau}_2, \end{aligned} \quad (28)$$

$$\begin{aligned} V_{PP-P^*P^*}^v &= \frac{1}{3} (\lambda g_V)^2 [-2\vec{\epsilon}^* \cdot \vec{\epsilon}^* D(r; m_v) \\ &+ 2\vec{\epsilon}^* \cdot \vec{\epsilon}^* C(r; m_v) - S_{\epsilon^* \epsilon^*} T(r; m_v)] \vec{\tau}_1 \cdot \vec{\tau}_2, \end{aligned} \quad (29)$$

$$\begin{aligned}
 V_{P^*P^*-P^*P^*}^v &= \left(\frac{\beta g_V}{2m_v}\right)^2 C(r; m_v) \vec{\tau}_1 \cdot \vec{\tau}_2 \\
 &+ \frac{1}{3}(\lambda g_V)^2 [-2\vec{T} \cdot \vec{T} D(r; m_v) \\
 &+ 2\vec{T} \cdot \vec{T} C(r; m_v) - S_{TT} T(r; m_v)] \vec{\tau}_1 \cdot \vec{\tau}_2;
 \end{aligned} \quad (30)$$

(iii) σ :

$$V_{PP-PP}^\sigma = -\left(\frac{g_s}{m_\sigma}\right)^2 C(r; m_\sigma), \quad (31)$$

$$V_{PP^*-PP^*}^\sigma = -\left(\frac{g_s}{m_\sigma}\right)^2 C(r; m_\sigma), \quad (32)$$

$$V_{P^*P^*-P^*P^*}^\sigma = -\left(\frac{g_s}{m_\sigma}\right)^2 C(r; m_\sigma), \quad (33)$$

where we adopt a static approximation, which means that energy transfers are neglected. The potentials considering an energy transfer have been done in Ref. [22]. In the following, we ignore the $D(r)$ term, which implies the delta function, because we focus on the long-range and middle-range parts of the meson exchange forces. ϵ^μ is the polarization vector, and \vec{T} is the spin-one operator, which are defined by

$$\epsilon^{(0)\mu} = (0, 0, 0, 1), \quad (34)$$

$$\epsilon^{(\pm)\mu} = \frac{1}{\sqrt{2}}(0, 1, \pm i, 0), \quad (35)$$

$$\vec{T} = -i\vec{\epsilon}^* \times \vec{\epsilon}, \quad (36)$$

respectively. $S_{12}(\hat{q}) = S_{\mathcal{O}_1\mathcal{O}_2}(\hat{q})$ is the tensor operator defined by

$$S_{12}(\hat{q}) = S_{\mathcal{O}_1\mathcal{O}_2}(\hat{q}) = 3(\vec{\mathcal{O}}_1 \cdot \hat{q})(\vec{\mathcal{O}}_2 \cdot \hat{q}) - \vec{\mathcal{O}}_1 \cdot \vec{\mathcal{O}}_2, \quad (37)$$

where $\hat{q} = \vec{q}/|\vec{q}|$. $C(r; m)$ and $T(r; m)$ are the central and the tensor potentials, respectively, which are defined by

$$C(r; m) = \int \frac{d^3q}{(2\pi)^3} \frac{m^2}{\vec{q}^2 + m^2} e^{i\vec{q}\cdot\vec{r}} F(\vec{q}; m)^2, \quad (38)$$

$$S_{12}(r)T(r; m) = \int \frac{d^3q}{(2\pi)^3} S_{12}(\hat{q}) \frac{-\vec{q}^2}{\vec{q}^2 + m^2} e^{i\vec{q}\cdot\vec{r}} F(\vec{q}; m)^2, \quad (39)$$

respectively. Here, we use

$$F(\vec{q}; m) = \frac{\Lambda^2 - m^2}{\Lambda^2 + \vec{q}^2} \quad (40)$$

as the form factor $F(\vec{q}; m)$ in order to consider a hadron size, where Λ is a cutoff parameter. Inserting this form factor into Eqs. (38) and (39), we obtain the central and the tensor functions:

$$C(r; m) = \frac{m^2}{4\pi} \left[\frac{e^{-mr}}{r} - \frac{e^{-\Lambda r}}{r} - \frac{\Lambda^2 - m^2}{2\Lambda} e^{-\Lambda r} \right], \quad (41)$$

$$\begin{aligned}
 T(r; m) &= \frac{1}{4\pi} (3 + 3mr + m^2 r^2) \frac{e^{-mr}}{r^3} \\
 &- \frac{1}{4\pi} (3 + 3\Lambda r + \Lambda^2 r^2) \frac{e^{-\Lambda r}}{r^3} \\
 &+ \frac{1}{4\pi} \frac{m^2 - \Lambda^2}{2} (1 + \Lambda r) \frac{e^{-\Lambda r}}{r}.
 \end{aligned} \quad (42)$$

We solve the Schrödinger equation in order to obtain the binding energy, wave functions, and mixing ratios. Then, let us show the Hamiltonian below:

$$H_{I(J^P)} = K_{I(J^P)} + \sum_{\text{boson}=\pi,\rho,\omega,\sigma} V_{\text{boson},I(J^P)}^{\text{HM}}, \quad (43)$$

where $K_{I(J^P)}$ is the kinetic energy and $V_{\text{boson},I(J^P)}^{\text{HM}}$ is the OBEP in HMB.

III. NUMERICAL RESULTS

In this section, we show the numerical results. First, we discuss the doubly charmed tetraquark T_{cc} . The cutoff parameter Λ is determined to reproduce the empirical binding energy of T_{cc} with $0(1^+)$. We study the properties of the $0(1^+)$ state and also the possible existence of the bound states of T_{cc} with other quantum numbers. Second, we discuss the doubly bottom tetraquark T_{bb} with given $I(J^P)$. Finally, we consider T_{QQ} in the HQL in order to see the HQS multiplets of the doubly heavy tetraquark. In Table I, we show the masses of mesons and the parameters used in this research. Here, the value of the coupling constant of a σ meson g_s is uncertainly. In this work, we use

TABLE I. The masses of mesons and the parameters [44–47].

Masses		Parameters	
m_π	138 MeV	g	0.59
m_ρ	770 MeV	g_V	$\frac{m_\rho}{\sqrt{2}f_\pi}$
m_ω	782 MeV	β	0.9
m_σ	500 MeV	λ	0.56 GeV ⁻¹
m_D	1868 MeV	g_s	3.4
m_{D^*}	2009 MeV		
m_B	5279 MeV		
m_{B^*}	5325 MeV		

$g_s = 3.4$, which is determined to be one-third of the coupling constant of a nucleon and a σ meson [44]. We also vary the value of g_s and discuss the g_s dependence of results.

A. Doubly charmed tetraquark T_{cc}

1. $I(J^P) = 0(1^+)$

As mentioned above, the pseudoscalar and vector mesons are degenerate in the HQL. Here, we consider the heavy pseudoscalar meson D and the heavy vector meson D^* , both of which include a charm quark. The mass difference between D and D^* is approximately 140 MeV. Then, we consider D and D^* as the HQS doublet. Thus, the threshold energies of DD , DD^* , and D^*D^* channels are

approximately degenerate. We consider these channels coupled by the one-boson exchange interactions. Let us show the possible channels for the $I(J^P) = 0(1^+)$ state $\psi_{0(1^+)}^{\text{HM}}$:

$$\psi_{0(1^+)}^{\text{HM}} = \begin{pmatrix} |[PP^*]_-(^3S_1)\rangle \\ |[PP^*]_-(^3D_1)\rangle \\ |P^*P^*(^3S_1)\rangle \\ |P^*P^*(^3D_1)\rangle \end{pmatrix}, \quad (44)$$

where we use the notations $[PP^*]_{\pm} = \frac{1}{\sqrt{2}}(PP^* \pm P^*P)$.

Also, we calculate the kinetic energy $K_{0(1^+)}$ and potential energies $V_{\text{boson},0(1^+)}^{\text{HM}}$:

$$K_{0(1^+)} = \text{diag} \left(-\frac{1}{2\mu_{PP^*}} \Delta_0, -\frac{1}{2\mu_{PP^*}} \Delta_2, -\frac{1}{2\mu_{P^*P^*}} \Delta_0 + \Delta m_{PP^*}, -\frac{1}{2\mu_{P^*P^*}} \Delta_2 + \Delta m_{PP^*} \right), \quad (45)$$

$$V_{\pi,0(1^+)}^{\text{HM}} = \begin{pmatrix} -C_{\pi} & \sqrt{2}T_{\pi} & 2C_{\pi} & \sqrt{2}T_{\pi} \\ \sqrt{2}T_{\pi} & -C_{\pi} - T_{\pi} & \sqrt{2}T_{\pi} & 2C_{\pi} - T_{\pi} \\ 2C_{\pi} & \sqrt{2}T_{\pi} & -C_{\pi} & \sqrt{2}T_{\pi} \\ \sqrt{2}T_{\pi} & 2C_{\pi} - T_{\pi} & \sqrt{2}T_{\pi} & -C_{\pi} - T_{\pi} \end{pmatrix}, \quad (46)$$

$$V_{v,0(1^+)}^{\text{HM}} = \begin{pmatrix} C'_v - 2C_v & -\sqrt{2}T_v & 4C_v & -\sqrt{2}T_v \\ -\sqrt{2}T_v & C'_v - 2C_v + T_v & -\sqrt{2}T_v & 4C_v + T_v \\ 4C_v & -\sqrt{2}T_v & C'_v - 2C_v & -\sqrt{2}T_v \\ -\sqrt{2}T_v & 4C_v + T_v & -\sqrt{2}T_v & C'_v - 2C_v + T_v \end{pmatrix}, \quad (47)$$

$$V_{\sigma,0(1^+)}^{\text{HM}} = \begin{pmatrix} C_{\sigma} & 0 & 0 & 0 \\ 0 & C_{\sigma} & 0 & 0 \\ 0 & 0 & C_{\sigma} & 0 \\ 0 & 0 & 0 & C_{\sigma} \end{pmatrix}, \quad (48)$$

where

$$\mu_{P^{(*)}P^{(*)}} = \frac{m_{P^{(*)}}m_{P^{(*)}}}{m_{P^{(*)}} + m_{P^{(*)}}}, \quad (49)$$

$$\Delta_l = \frac{d^2}{dr^2} - \frac{l(l+1)}{r^2}, \quad (50)$$

$$\Delta m_{PP^*} = m_{P^*} - m_P, \quad (51)$$

$$C_{\pi} = \frac{1}{3} \left(\frac{g}{2f_{\pi}} \right)^2 C(r; m_{\pi}) \vec{\tau}_1 \cdot \vec{\tau}_2, \quad (52)$$

$$T_{\pi} = \frac{1}{3} \left(\frac{g}{2f_{\pi}} \right)^2 T(r; m_{\pi}) \vec{\tau}_1 \cdot \vec{\tau}_2, \quad (53)$$

$$C'_v = \left(\frac{\beta g_V}{2m_v} \right)^2 C(r; m_v) \vec{\tau}_1 \cdot \vec{\tau}_2, \quad (54)$$

$$C_v = \frac{1}{3} (\lambda g_V)^2 C(r; m_v) \vec{\tau}_1 \cdot \vec{\tau}_2, \quad (55)$$

$$T_v = \frac{1}{3} (\lambda g_V)^2 T(r; m_v) \vec{\tau}_1 \cdot \vec{\tau}_2, \quad (56)$$

$$C_{\sigma} = - \left(\frac{g_s}{m_{\sigma}} \right)^2 C(r; m_{\sigma}). \quad (57)$$

For an omega meson, we remove $\vec{\tau}_1 \cdot \vec{\tau}_2$, because the isospin of an omega meson is 0.

First, we consider only the one- π exchange force in the $D^{(*)}D^{(*)}$ molecule. In this case, no bound state of T_{cc} with $0(1^+)$ exists for reasonable Λ . However, considering the OBEP as the interaction of a hadronic molecule, we obtain the bound state of T_{cc} with $0(1^+)$ as shown in Fig. 1. The binding energy of T_{cc} reported by LHCb, 0.273 MeV [9], is obtained for $\Lambda = 1069.8$ MeV. The bound state properties with $\Lambda = 1069.8$ MeV, the wave functions, the mixing ratios, and the root-mean square distance (rms), are shown in Fig. 2 and Table II. Here, the mixing ratios f and the rms are defined by

$$f(\text{channel}) = \langle \chi_{\text{channel}} | \chi_{\text{channel}} \rangle,$$

$$\sqrt{\langle r^2 \rangle} = \sqrt{\langle \chi | r^2 | \chi \rangle},$$

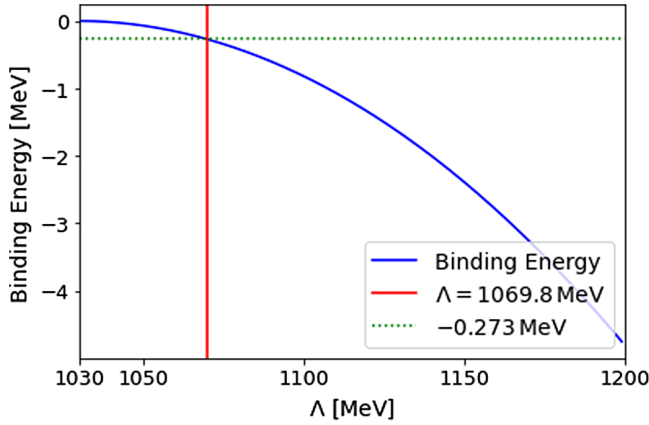


FIG. 1. The binding energy of T_{cc} with $0(1^+)$ for $\Lambda = 1030$ – 1200 MeV. The vertical solid line indicates $\Lambda = 1069.8$ MeV and the horizontal dotted line does -0.273 MeV, which is the experimental value of the T_{cc} binding energy [9].

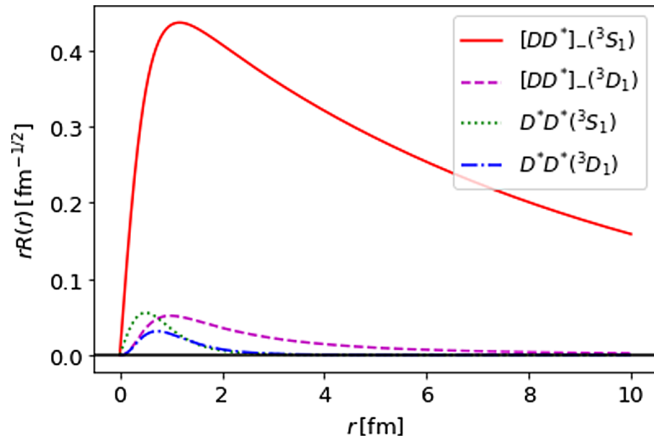


FIG. 2. The wave function of each channel for T_{cc} with $0(1^+)$. The solid, dashed, dotted, and dash-dotted lines show the wave functions of $[DD^*]_-(^3S_1)$, $[DD^*]_-(^3D_1)$, $D^*D^*(^3S_1)$, and $D^*D^*(^3D_1)$ channels, respectively.

TABLE II. The mixing ratios of each channel and the rms for T_{cc} with $0(1^+)$ where $\Lambda = 1069.8$ MeV.

Mixing ratio and rms	
$[DD^*]_-(^3S_1)$	99.2%
$[DD^*]_-(^3D_1)$	0.467%
$D^*D^*(^3S_1)$	0.229%
$D^*D^*(^3D_1)$	0.0854%
rms	6.43 fm

where $\chi = rR(r)$ and χ_{channel} is the wave function of a channel. Also, the potential expectation values of the OBEP are shown in Fig. 3 as like matrices. Each component in Fig. 3 shows the expectation values of corresponding potential component in Eqs. (46)–(48). For example, 0.47 in Fig. 3(a) is the expectation value of the (1,1) component of V^π . Our analyses show that considering only the OPEP cannot earn the attractive force necessary to bind T_{cc} . However, we get the bound state of T_{cc} in the case of OBEP. In fact, Fig. 3(d) shows that the (1,1) component of V^σ generates the strongest attraction among all potential expectation values, indicating that the exchange of a σ meson is the most significant. Also, the (1,2), (2,1), (1,4), and (4,1) components of the OPEP tensor term in Fig. 3(a) and the (1,1), (1,3), and (3,1) components of the ρ exchange potential in Fig. 3(b) are important to produce an attraction. Thus, the bound states of T_{cc} with $0(1^+)$ are obtained in the case of the OBEP.

Finally, we note that a similar study with the on-shell pion exchange was done in Ref. [22]. We find that the bound state properties obtained in Ref. [22] and in the current study are qualitatively the same. In both studies, the cutoff parameter of the one-boson exchange potentials is a free parameter and able to be determined within the reasonable range of values to reproduce the empirical binding energy of T_{cc} .

Next, we vary the value of the sigma coupling g_s by $\pm 10\%$ because of the uncertainty of g_s and study g_s dependence of the binding energy for $\Lambda = 1069.8$ MeV, as shown in Fig. 4. This analysis shows that we can obtain the bound state of T_{cc} for $g_s \geq 3.22$, and the binding energy of T_{cc} for $\Lambda = 1069.8$ MeV varies greatly when we vary g_s . This analysis implies the binding energy highly depends on g_s . Furthermore, we also investigate g_s dependence of the cutoff parameter Λ to reproduce the experimental binding energy of T_{cc} as shown in Fig. 5. This result shows that, even if g_s is varied as $3.06 \leq g_s \leq 3.74$, we obtain the bound state with the empirical binding energy having the reasonable cutoff as $1001.3 \text{ MeV} \leq \Lambda \leq 1147.1 \text{ MeV}$.

2. Other quantum numbers

In this section, we study T_{cc} with other quantum numbers, $0(0^-)$, $0(1^-)$, $1(0^+)$, $1(0^-)$, $1(1^+)$, and $1(1^-)$.

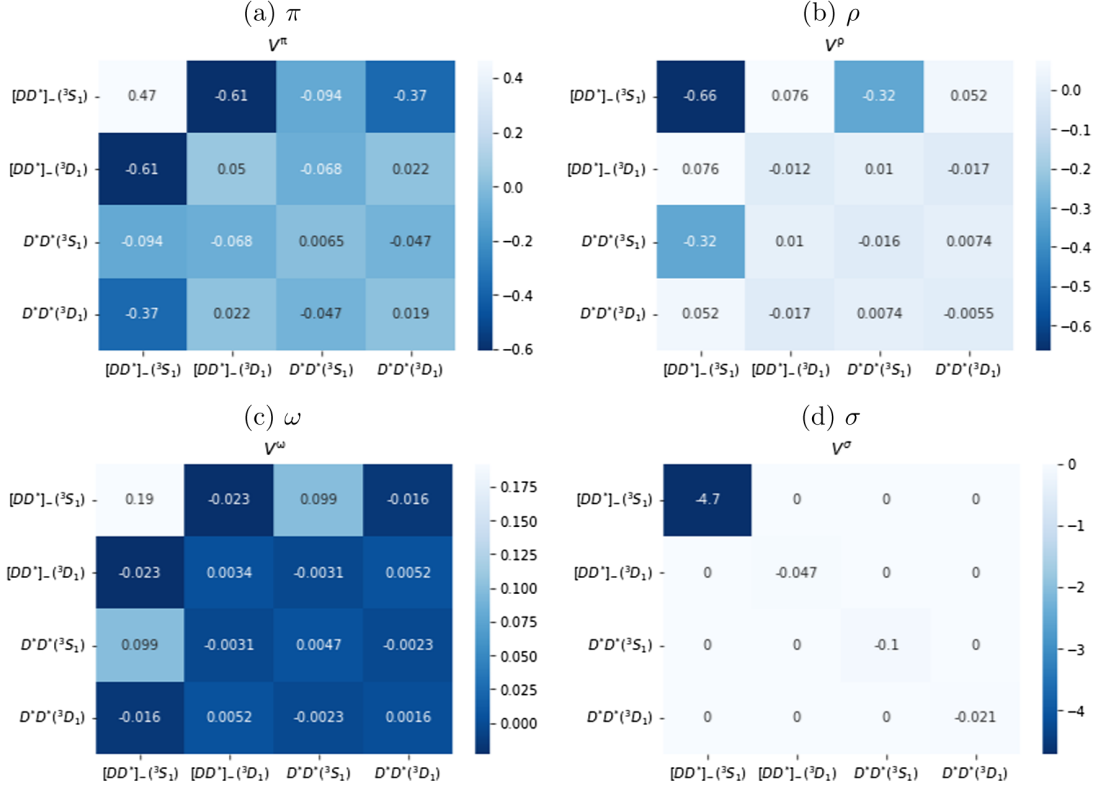


FIG. 3. The expectation values of the OBEP for T_{cc} with $0(1^+)$. The value is given in units of MeV.

The possible channels of these quantum numbers are shown in Table III, and the potential matrices are shown in Appendix A. Here, we consider the case where $g_s = 3.06, 3.4, 3.74$. We solve the Schrödinger equations for these quantum numbers, but we obtain no bound states of T_{cc} with other quantum numbers, as shown in Table IV.

B. Doubly bottom tetraquark T_{bb}

In this section, we consider T_{bb} as a hadronic molecule of B and B^* , including two bottom quarks. In Sec. III A, we consider D and D^* as a HQS doublet, because the mass difference of D and D^* is smaller than those in the light quark sectors. Similarly, we think of B and B^* as a HQS doublet, since the mass difference of B and B^* is approximately 45 MeV, and the $BB^* - B^*B^*$ channel-coupling effect is expected to be enhanced.

1. $I(J^P) = 0(1^+)$

First, we discuss the T_{bb} with $0(1^+)$ as a hadronic molecule whose interaction is only π exchange force. By solving the Schrödinger equation of the $B^{(*)}B^{(*)}$ two-body system, we obtain the bound state for T_{bb} with $0(1^+)$, while T_{cc} does not bind only by the OPEP with the reasonable cutoff as discussed in the previous section. The binding energies with various cutoff Λ are shown in Fig. 6, where the binding energy of T_{bb} increases as Λ increases. The analysis with only the OPEP indicates that it is highly likely

that the bound state of T_{bb} exists, because additional attractions from the short-range forces are also expected as discussed below.

We also consider the case where the interaction of a hadronic molecule is the OBEP. We use the same cutoff of T_{cc} , $\Lambda = 1069.8$ MeV, determined in the previous section, and calculate the binding energy of T_{bb} with $0(1^+)$. As a result, we find that the binding energy is 46.0 MeV and also get wave functions, mixing ratios, and the rms as shown in Fig. 7 and Table V. These results show that the channel of

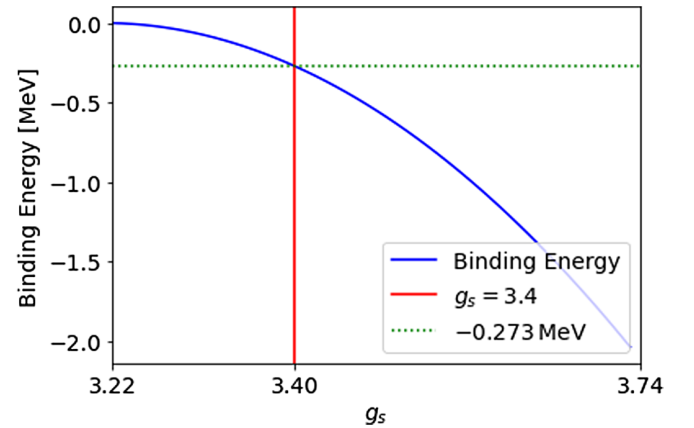


FIG. 4. The relation of the binding energy of T_{cc} and g_s . The vertical solid line indicates $g_s = 3.4$ and the horizontal dotted line does -0.273 MeV, which is the experimental value.

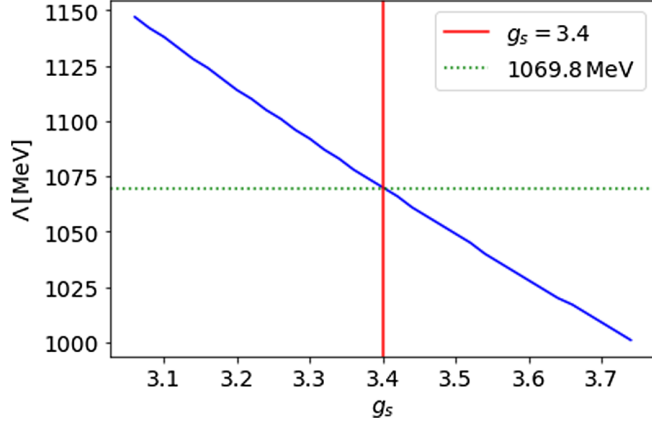


FIG. 5. The relation between g_s and Λ which reproduces the experimental value of the T_{cc} binding energy. The vertical solid and horizontal dotted lines indicate $g_s = 3.4$ and $\Lambda = 1069.8$ MeV, respectively.

$B^*B^*(^3S_1)$ is important in addition to the one of $[BB^*]_-(^3S_1)$ unlike T_{cc} . The importance of the $B^*B^*(^3S_1)$ channel is also seen in the potential expectation values in Fig. 8. The expectation values of the one- σ exchange potential in Fig. 8(d) show that the dominant

TABLE III. The possible channels for each quantum number. We use the notation $[PP^*]_{\pm} = \frac{1}{\sqrt{2}}(PP^* \pm P^*P)$ and $^{2S+1}L_J$, where S is the total spin, L is the orbital angular momentum, and J is the total angular momentum [16].

$I(J^P)$	Channels
$0(0^-)$	$[PP^*]_+(^3P_0)$
$0(1^+)$	$[PP^*]_-(^3S_1), [PP^*]_-(^3D_1), P^*P^*(^3S_1), P^*P^*(^3D_1)$
$0(1^-)$	$PP(^1P_1), [PP^*]_+(^3P_1), P^*P^*(^1P_1), P^*P^*(^5P_1), P^*P^*(^5F_1)$
$1(0^+)$	$PP(^1S_0), P^*P^*(^1S_0), P^*P^*(^5D_0)$
$1(0^-)$	$[PP^*]_-(^3P_0), P^*P^*(^3P_0)$
$1(1^+)$	$[PP^*]_+(^3S_1), [PP^*]_+(^3D_1), P^*P^*(^5D_1)$
$1(1^-)$	$[PP^*]_-(^3P_1), P^*P^*(^3P_1)$

TABLE IV. The binding energies (B) of T_{cc} with given $I(J^P)$. In the table, $-B$ is displayed in units of MeV. The dependence of the binding energy on Λ and g_s is shown. The set of (g_s, Λ) is determined to reproduce the experimental value of T_{cc} as shown in Fig. 5.

g_s	3.06	3.4	3.74
Λ [MeV]	1147.1	1069.8	1001.3
$0(0^-)$
$0(1^+)$	-0.273	-0.273	-0.273
$0(1^-)$
$1(0^+)$
$1(0^-)$
$1(1^+)$
$1(1^-)$

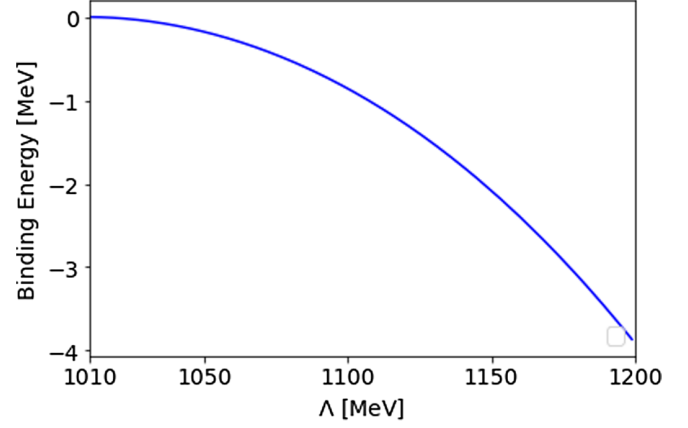


FIG. 6. The relation between the binding energy of T_{bb} with $0(1^+)$ and Λ for OPEP.

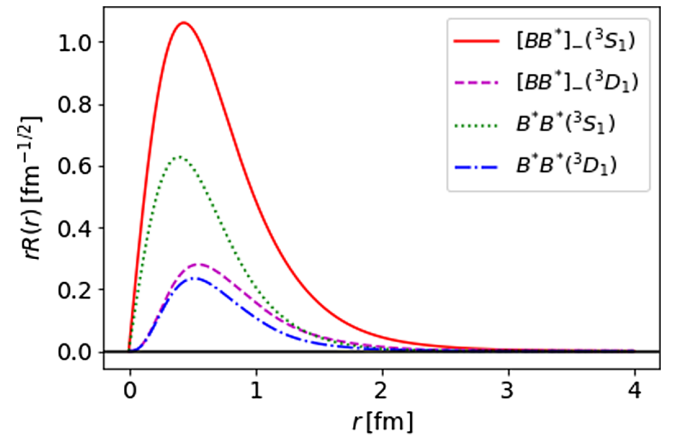


FIG. 7. The wave function of each channel for T_{bb} with $0(1^+)$. The solid, dashed, dotted, and dash-dotted lines show the wave functions of $[BB^*]_-(^3S_1)$, $[BB^*]_-(^3D_1)$, $B^*B^*(^3S_1)$, and $B^*B^*(^3D_1)$ channels, respectively.

component is given by the (1,1) component, which is the same in the case of T_{cc} as shown in Fig. 3(d). In addition, the (3,3) component in Fig. 8(d) also produces the strong attraction, whereas the corresponding component of T_{cc} is not important. The other meson exchanges also have an important role to generate the attraction. The (1,2), (2,1), (1,4), and (4,1) components in Fig. 8(a) are important, which implies the tensor force of the one-pion exchange contributes to bind T_{bb} just like the case of T_{cc} . The (1,3)

TABLE V. The mixing ratios of each channel and rms for T_{bb} with $0(1^+)$ where $\Lambda = 1069.8$ MeV.

Mixing ratio and rms	
$[BB^*]_-(^3S_1)$	70.7%
$[BB^*]_-(^3D_1)$	4.71%
$B^*B^*(^3S_1)$	21.6%
$B^*B^*(^3D_1)$	3.00%
rms	0.620 fm

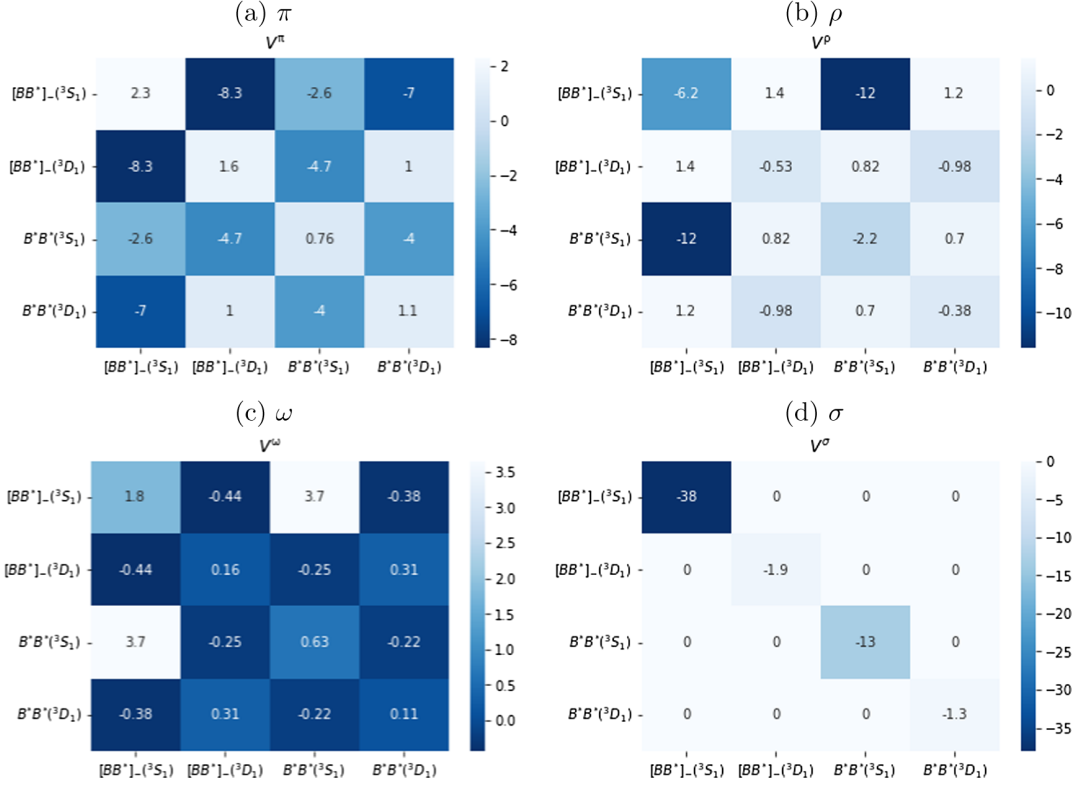


FIG. 8. The expectation values of the OBEP for T_{bb} with $0(1^+)$. The value is given in units of MeV.

and (3,1) components in Fig. 8(b) primarily contributed by the ρ meson exchange are important to generate the attraction. These are because the mass difference of BB^* and B^*B^* is smaller than that of DD^* and D^*D^* . Therefore, the channels $[BB^*]_-$ and B^*B^* are more coupled with each other. However, we emphasize that, similar to T_{cc} , the σ meson exchange potential has the dominant contribution to earn the attractive force binding the T_{bb} .

2. Other quantum numbers

In this section, we discuss T_{bb} with given $I(J^P)$. The obtained binding energies are summarized in Table VI. As a result, many bound states of T_{bb} appear. Table VI shows the (g_s, Λ) dependence of the T_{bb} binding energies, where the

TABLE VI. The binding energies of T_{bb} with given $I(J^P)$. The same convention as Table IV is used.

g_s	3.06	3.4	3.74
Λ [MeV]	1147.1	1069.8	1001.3
$0(0^-)$	-30.7	-24.4	-19.2
$0(1^+)$	-56.2	-46.0	-37.9
$0(1^-)$
$1(0^+)$	-3.70	-7.23	-10.8
$1(0^-)$
$1(1^+)$	-0.0254	-2.46	-6.98
$1(1^-)$

parameter set (g_s, Λ) is determined to reproduce the empirical binding energy of T_{cc} as shown in Table IV and Fig. 5. Examining the (g_s, Λ) dependence is useful to understand the natures of the different isospin states. Table VI shows that, as g_s increases and simultaneously Λ decreases (the σ exchange is enhanced, while the other meson exchanges are suppressed), the bound states of T_{bb} with the isospin $I = 0$ become shallower, while the ones with the isospin $I = 1$ become deeper. The difference between the isospin states is caused by the isospin factor $\vec{\tau}_1 \cdot \vec{\tau}_2$ of the isovector π, ρ exchange potentials:

$$\vec{\tau}_1 \cdot \vec{\tau}_2 = \begin{cases} -3 & \text{for } I = 0, \\ 1 & \text{for } I = 1. \end{cases}$$

Since the strength of the $\vec{\tau}_1 \cdot \vec{\tau}_2$ factor of the $I = 0$ channel is 3 times larger than the one of the $I = 1$ channel, the π, ρ exchange potentials have a non-negligible role in the $I = 0$ bound states, while it is suppressed in the case of $I = 1$. It can also be seen in the (g_s, Λ) dependence of the energy expectation values in Table VII. For $0(1^+)$, the off-diagonal components are drastically reduced as Λ decreases, which are mainly contributed by the isovector π, ρ exchange potentials. The reduction of the expectation value is also seen for the $0(0^-)$ state. On the other hand, the expectation values of the $I = 1$ bound states are more sensitive to the change of g_s , being the coupling constant of the σ exchange in the diagonal components.

TABLE VII. Dependence of the energy expectation value of T_{bb} for given $I(J^P)$ on the parameters (g_s, Λ) . Only the important components are shown in the table. The expectation value is given in units of MeV.

	g_s	3.06	3.40	3.74	
0(1 ⁺)	Λ [MeV]	1147.1	1069.8	1001.3	
	(1, 1)	-39	-40	-41	
	(1, 2)	-8.6	-7.3	-6.2	
	(2, 1)				
	(1, 3)	-16	-11	-6.7	
	(3, 1)				
	(1, 4)	-7.4	-6.2	-5.1	
	(4, 1)				
	(2, 3)	-5.5	-4.1	-2.9	
	(3, 2)				
0(0 ⁻)	V_{total}	-108	-90.6	-75.7	
	1(0 ⁺)	(1, 1)	-13	-22	-30
		(1, 2)	-2.6	-1.8	-0.99
		(2, 1)			
(1, 3)		-0.55	-0.74	-0.85	
1(1 ⁺)	(3, 1)				
	(2, 2)	-1.9	-1.3	-0.72	
	(1, 1)	-0.72	-10	-21	
	(1, 2)	-0.057	-0.4	-0.51	
	(2, 1)				
	(1, 3)	-0.095	-0.76	-1.1	
	(3, 1)				

C. Doubly heavy tetraquarks T_{QQ} in the heavy quark limit

1. Light-cloud basis

Until now, we have discussed the hadronic molecules of P and P^* as T_{cc} and T_{bb} . In this section, by introducing the LCB, we consider the HQS multiplet structure of the molecules in the HQL. As discussed in Refs. [40–42], HQS and LCB are useful to classify bound states by the heavy quark spin and total angular momentum of the light cloud.

We can obtain the LCB by implementing the unitary transformation to the HMB [40–42]:

$$\begin{aligned}
 & \left[L \left[[S_{Q_1} S_{q_1}]_{S_1} [S_{Q_2} S_{q_2}]_{S_2} \right]_S \right]_J \\
 & \rightarrow \left[[S_{Q_1} S_{Q_2}]_{S_Q} \left[L [S_{q_1} S_{q_2}]_{S_q} \right]_{J_l} \right]_J, \quad (58)
 \end{aligned}$$

where L is the orbital momentum and S_{Q_i} and S_{q_i} ($i = 1, 2$) are the spins of the heavy quark Q_i and light antiquark q_i of the heavy meson $P_i^{(*)} = Q_i \bar{q}_i$ with the spin S_i , respectively. S and J are the total spin and angular momentum of two heavy mesons, S_Q and S_q are the spins of the heavy diquark and the light antidiquark, and J_l is the spin of the light cloud. This transformation leads to find the spin structures including the diquark spins inside the hadronic molecule, which we cannot see in the HMB.

Here, we implement this unitary transformation from the HMB to the LCB for 0(1⁺) as an example. First, the transformation from the wave function in the HMB, $\psi_{0(1^+)}^{\text{HM}}$, to that in the LCB, $\psi_{0(1^+)}^{\text{LC}}$, is given by

$$\begin{aligned}
 \psi_{0(1^+)}^{\text{LC}} &= U_{0(1^+)}^{-1} \psi_{0(1^+)}^{\text{HM}} \\
 &= \begin{pmatrix} \left| \left[[QQ]_1 [S[\bar{q}\bar{q}]_{0,0}]_1 \right] \right\rangle \\ \left| \left[[QQ]_0 [S[\bar{q}\bar{q}]_{1,1}]_1 \right] \right\rangle \\ \left| \left[[QQ]_0 [D[\bar{q}\bar{q}]_{1,1}]_1 \right] \right\rangle \\ \left| \left[[QQ]_1 [D[\bar{q}\bar{q}]_{0,2}]_1 \right] \right\rangle \end{pmatrix}, \quad (59) \\
 U_{0(1^+)} &= \begin{pmatrix} -\frac{1}{\sqrt{2}} & \frac{1}{\sqrt{2}} & 0 & 0 \\ 0 & 0 & \frac{1}{\sqrt{2}} & -\frac{1}{\sqrt{2}} \\ \frac{1}{\sqrt{2}} & \frac{1}{\sqrt{2}} & 0 & 0 \\ 0 & 0 & \frac{1}{\sqrt{2}} & \frac{1}{\sqrt{2}} \end{pmatrix}, \quad (60)
 \end{aligned}$$

where $U_{0(1^+)}$ is the unitary matrix determined by the Clebsch-Gordan coefficient. Second, using $U_{0(1^+)}$, we transform the potential matrices $V_{\text{boson},0(1^+)}^{\text{HM}}$ in the HMB to $V_{\text{boson},0(1^+)}^{\text{LC}}$ in the LCB. Then we obtain the block-diagonal potential matrices:

$$\begin{aligned}
 V_{\pi,0(1^+)}^{\text{LC}} &= U_{0(1^+)}^{-1} V_{\pi,0(1^+)}^{\text{HM}} U_{0(1^+)} \\
 &= \begin{pmatrix} -3C_\pi & 0 & 0 & 0 \\ 0 & C_\pi & 2\sqrt{2}T_\pi & 0 \\ 0 & 2\sqrt{2}T_\pi & C_\pi - 2T_\pi & 0 \\ 0 & 0 & 0 & -3C_\pi \end{pmatrix}, \quad (61)
 \end{aligned}$$

$$V_{v,0(1^+)}^{\text{LC}} = U_{0(1^+)}^{-1} V_{v,0(1^+)}^{\text{HM}} U_{0(1^+)} = \left(\begin{array}{c|cc|c} C'_v - 6C_v & 0 & 0 & 0 \\ \hline 0 & C'_v + 2C_v & -2\sqrt{2}T_v & 0 \\ \hline 0 & -2\sqrt{2}T_v & C'_v + 2C_v + 2T_v & 0 \\ \hline 0 & 0 & 0 & C'_v - 6C_v \end{array} \right), \quad (62)$$

$$V_{\sigma,0(1^+)}^{\text{LC}} = U_{0(1^+)}^{-1} V_{\sigma,0(1^+)}^{\text{HM}} U_{0(1^+)} = \left(\begin{array}{c|cc|c} C_\sigma & 0 & 0 & 0 \\ \hline 0 & C_\sigma & 0 & 0 \\ \hline 0 & 0 & C_\sigma & 0 \\ \hline 0 & 0 & 0 & C_\sigma \end{array} \right). \quad (63)$$

Since states with different S_Q or J_l are decoupled in the HQL, the off-diagonal components mixing these states vanish in the LCB. Hence, if a bound state is obtained, it is an eigenstate corresponding to one of the components which is characterized by S_Q and J_l . Thus, these $\psi_{l(J^p)}^{\text{LC}}$ and matrices $V_{\text{boson},0(1^+)}^{\text{LC}}$ enable us to find the spin structures of the diquark.

We note that the matrix elements of the block-diagonal potential coincide with those of the meson exchange potential between corresponding light quarks. In this study, we employ only the light meson exchange interactions which work between light quarks and the rest heavy quark is a spectator. Thus, using the transformation from the HMB to LCB, the potentials between heavy mesons are rewritten as those between the light quarks inside the heavy mesons.

The diquark spins S_Q and J_l also indicate the HQS multiplet structure of bound states. We define that states with the same (S_Q, J_l) but with different J form an HQS multiplet, where $\vec{J} = \vec{S}_Q + \vec{J}_l$ [40–42]. For instance, the first component of Eq. (59) has $S_Q = 1$ and $J_l = 0$. Since only $J = 1$ can be generated from $S_Q = 1$ and $J_l = 0$, the bound state for this component should belong to the HQS singlet, and, hence, it has no HQS partner.¹ Similarly, the coupled channel system of the second and third components has $S_Q = 0$ and $J_l = 1$. Thus, the bound state is in the HQS singlet. Therefore, from the LCB of the $0(1^+)$ state,

we find that if there is a S -wave bound state, it belongs to the HQS singlet. On the other hand, the fourth component having $S_Q = 1$ and $J_l = 2$ with $L = 2$ may have the HQS partners with high J , because both S_Q and J_l are nonzero.

We also show an example of the unitary transformation for $0(0^-)$ and $0(1^-)$, where we can see the HQS multiplet structure of them. As seen in the case of $0(1^+)$ states, the light-cloud basis $\psi_{0(0^-)}^{\text{LC}}$ and $\psi_{0(1^-)}^{\text{LC}}$ and the one-boson exchange potential matrices $V_{\text{boson},0(0^-)}^{\text{LC}}$ and $V_{\text{boson},0(1^-)}^{\text{LC}}$ can be obtained under the unitary transformations as

$$\psi_{0(0^-)}^{\text{LC}} = \left(- \left| \left[[QQ]_1 [P[\bar{q}\bar{q}]_1]_1 \right]_0 \right\rangle \right), \quad (64)$$

$$\psi_{0(1^-)}^{\text{LC}} = U_{0(1^-)}^{-1} \psi_{0(1^-)}^{\text{HM}} = \left(\begin{array}{c} \left| \left[[QQ]_0 [P[\bar{q}\bar{q}]_0]_1 \right]_1 \right\rangle \\ \left| \left[[QQ]_1 [P[\bar{q}\bar{q}]_1]_0 \right]_1 \right\rangle \\ \left| \left[[QQ]_1 [P[\bar{q}\bar{q}]_1]_1 \right]_1 \right\rangle \\ \left| \left[[QQ]_1 [P[\bar{q}\bar{q}]_1]_2 \right]_1 \right\rangle \\ \left| \left[[QQ]_1 [F[\bar{q}\bar{q}]_1]_2 \right]_1 \right\rangle \end{array} \right), \quad (65)$$

$$V_{\pi,0(0^-)}^{\text{LC}} = (C_\pi + 2T_\pi), \quad (66)$$

$$V_{\pi,0(1^-)}^{\text{LC}} = U_{0(1^-)}^{-1} V_{\pi,0(1^-)}^{\text{HM}} U_{0(1^-)} = \left(\begin{array}{c|cc|cc} -3C_\pi & 0 & 0 & 0 & 0 \\ \hline 0 & C_\pi - 4T_\pi & 0 & 0 & 0 \\ \hline 0 & 0 & C_\pi + 2T_\pi & 0 & 0 \\ \hline 0 & 0 & 0 & C_\pi - \frac{2}{5}T_\pi & \frac{6\sqrt{6}}{5}T_\pi \\ \hline 0 & 0 & 0 & \frac{6\sqrt{6}}{5}T_\pi & C_\pi - \frac{8}{5}T_\pi \end{array} \right), \quad (67)$$

¹We note that, since $J = 1$, this state forms a spin triplet.

TABLE VIII. Energy eigenvalues E ($=-B$ with binding energies B) and mixing ratios of each channel for $0(1^+)$ in the HQL ($m_P = m_{P^*} = 5m_{B^*}$). The energy is given in units of MeV.

	E [MeV]	$[PP^*]_-$ (3S_1)	$[PP^*]_-$ (3D_1)	P^*P^* (3S_1)	P^*P^* (3D_1)
Ground	-162	41.9%	8.07%	41.9%	8.07%
1st	-77.4	38.9%	11.1%	38.9%	11.1%
2nd	-25.9	50.0%	0%	50.0%	0%
3rd	-25.4	37.2%	12.8%	37.2%	12.8%
4th	-3.07	37.3%	12.7%	37.3%	12.7%

 TABLE IX. Energy eigenvalues E ($=-B$ with binding energies B) for $0(0^-)$ in the HQL ($m_P = m_{P^*} = 5m_{B^*}$). The energy is given in units of MeV.

	E [MeV]
Ground	-141
1st	-60.1
2nd	-15.6
3rd	-0.796

where only the one-pion exchange potentials are shown as an example. Comparing the potential matrices in Eqs. (66) and (67) shows the same components, $C_\pi + 2T_\pi$, where their spin structures are also the same, $S_Q = 1$ and $J_l = 1$. It is also found for the other one-boson exchange matrices. Thus, the eigenstates of the corresponding Hamiltonian component in the $0(0^-)$ and $0(1^-)$ states are degenerate in the HQL and belong to the HQS multiplet. In addition, since a combination of $S_Q = 1$ and $J_l = 1$ generates $J = 0, 1, 2$, i.e., $S_Q \otimes J_l = 1 \otimes 1 = 0 \oplus 1 \oplus 2$, we also expect that the $0(2^-)$ state has the same component, and the corresponding components of $0(0^-)$, $0(1^-)$, and $0(2^-)$ belong to the same HQS triplet.

We note that the block diagonal nature of the Hamiltonian and the HQS multiplet appears because of the HQS in the HQL. In the finite mass region, however, a mass splitting of pseudoscalar and vector mesons violates the symmetry, and, hence, the block diagonal nature disappears. In fact, as we discuss later, the $0(0^-)$ and

 TABLE XI. Energy eigenvalues E ($=-B$ with binding energies B) and mixing ratios of each channel for $1(0^+)$ in the HQL ($m_P = m_{P^*} = 5m_{B^*}$). The energy is given in units of MeV.

	E [MeV]	$PP({}^1S_0)$	$P^*P^*({}^1S_0)$	$P^*P^*({}^5D_0)$
Ground	-87.0	25.0%	75.0%	0%
1st	-33.4	58.5%	19.5%	22.1%
2nd	-21.8	25.0%	75.0%	0%
3rd	-7.61	43.0%	14.3%	42.6%
4th	-0.561	25.0%	75.0%	0%

 TABLE XII. Energy eigenvalues E ($=-B$ with binding energies B) and mixing ratios of each channel for $1(1^+)$ in the HQL ($m_P = m_{P^*} = 5m_{B^*}$). The binding energy is given in units of MeV.

	E [MeV]	$[PP^*]_+({}^3S_1)$	$[PP^*]_+({}^3D_1)$	$P^*P^*({}^5D_1)$
Ground	-33.4	77.9%	5.52%	16.5%
1st	-7.61	57.4%	10.7%	32.0%

$0(1^-)$ bound states are degenerate, which have been already expected to belong to the same HQS multiplet in the HQL as seen in Eqs. (66) and (67). However, in the bottom sector, the $0(0^-)$ bound state is obtained while the $0(1^-)$ one is absent. Hence, the block diagonal nature of these states is broken in the finite mass region.

We also obtain the other $\psi_{I(J^P)}^{\text{LC}}$ and $V_{\text{boson}, I(J^P)}^{\text{LC}}$ summarized in Appendix B.

2. T_{QQ} in HQL and the spin structure

We calculate the binding energy of T_{QQ} with given $I(J^P)$ in the HQL. In fact, the Schrödinger equations for T_{QQ} cannot be solved numerically, because the reduced masses of the two mesons diverge. To demonstrate a computation in the HQL, we take $m_P = m_{P^*} = 5m_{B^*}$, which implies that the masses of the pseudoscalar meson and the vector meson are degenerate. Using these masses, we discuss the HQS multiplet structure for T_{cc} . These results are shown in Tables VIII–XIV.

 TABLE X. Energy eigenvalues E ($=-B$ with binding energies B) and mixing ratios of each channel for $0(1^-)$ in the HQL ($m_P = m_{P^*} = 5m_{B^*}$). The energy is given in units of MeV.

	E [MeV]	$PP({}^1P_1)$	$[PP^*]_+({}^3P_1)$	$P^*P^*({}^1P_1)$	$P^*P^*({}^5P_1)$	$P^*P^*({}^5F_1)$
Ground	-141	25.0%	25.0%	8.33%	41.7%	0%
1st	-104	32.4%	32.4%	10.8%	2.16%	22.3%
2nd	-60.1	25.0%	25.0%	8.33%	41.7%	0%
3rd	-38.7	30.4%	30.4%	10.1%	2.03%	27.1%
4th	-15.6	25.0%	25.0%	8.33%	41.7%	0%
5th	-6.40	29.8%	29.8%	9.93%	1.99%	28.5%
6th	-4.37	25.0%	0%	75.0%	0%	0%
7th	-0.796	25.0%	25.0%	8.33%	41.7%	0%

TABLE XIII. Energy eigenvalues E ($=-B$ with binding energies B) and mixing ratios of each channel for $1(0^-)$ in the HQL ($m_P = m_{P^*} = 5m_{B^*}$). The binding energy is given in units of MeV.

	E [MeV]	$[PP^*]_-(^3P_0)$	$P^*P^*(^3P_0)$
Ground	-42.5	50.0%	50.0%
1st	-33.9	50.0%	50.0%
2nd	-6.09	50.0%	50.0%
3rd	-4.27	50.0%	50.0%

TABLE XIV. Energy eigenvalues E ($=-B$ with binding energies B) and mixing ratios of each channel for $1(1^-)$ in the HQL ($m_P = m_{P^*} = 5m_{B^*}$). The binding energy is given in units of MeV.

	E [MeV]	$[PP^*]_-(^3P_1)$	$P^*P^*(^3P_1)$
Ground	-42.5	50.0%	50.0%
1st	-4.27	50.0%	50.0%

For the $0(1^+)$ state in the HQL, the result summarized in Table VIII shows that there are five bound states. However, the origin of these states is different, which is indicated by their mixing ratios. The mixing ratios f of the ground state and first, third, and fourth excited states in the HMB are

$$f([PP^*]_-(^3S_1)) : f(P^*P^*(^3S_1)) = 1 : 1,$$

$$f([PP^*]_-(^3D_1)) : f(P^*P^*(^3D_1)) = 1 : 1,$$

obtained as the S - D mixing states. These relations show that these bound states are composed of

$$\left(\begin{array}{c} \left| \left[[QQ]_0 [S[\bar{q}\bar{q}]_{11}]_1 \right]_1 \right\rangle \\ \left| \left[[QQ]_0 [D[\bar{q}\bar{q}]_{11}]_1 \right]_1 \right\rangle \end{array} \right) \quad (68)$$

components in Eq. (59) in the LCB. Thus, we also find that the diquark spins of these bound states are $S_Q = 0$ and $S_q = 1$. On the other hand, the mixing ratio of the remaining state, the second excited state, is

$$f([PP^*]_-(^3S_1)) = f(P^*P^*(^3S_1)) = 50\%,$$

$$f([PP^*]_-(^3D_1)) = f(P^*P^*(^3D_1)) = 0\%,$$

having no D -wave state. Therefore, this bound state is built by the $\left| \left[[QQ]_1 [S[\bar{q}\bar{q}]_0]_0 \right]_1 \right\rangle$ component in Eq. (59) in the LCB, where the diquark spins are obtained by $S_Q = 1$ and $S_q = 0$.

These results are obtained in the HQL, while in experiments, it is possible to observe doubly heavy tetraquarks with finite quark mass. Next, by reducing the heavy meson

masses toward to the bottom and charmed meson regions, we connect the results of T_{QQ} in the HQL, T_{bb} , and T_{cc} where the HQS is not held exactly in the finite quark mass region. Figure 9 shows the heavy vector meson mass dependence of $\Delta m_P = m_{P^*} - m_P$. By fitting the experimental data of the meson masses, we obtain $\Delta m_P = 2.00 \times 10^6 / m_{P^*}^{1.25}$ as a function of m_{P^*} [48]. By using this function, we obtain the mass dependence of the energy eigenvalue and mixing ratios of T_{QQ} with each quantum number, as shown in Figs. 10–13. The curves in these figures are continuous; thus, we can see the origin of T_{cc} and T_{bb} in the HQL. As for $0(1^+)$, Fig. 10 shows that the origin of T_{cc} and T_{bb} bound states obtained in this paper is the ground state of T_{QQ} in the HQL with the spin structures $S_Q = 0, S_q = 1$, indicating that this T_{QQ} state belongs to the HQS singlet. Thus, the T_{cc} state reported by LHCb is originated from the HQS singlet state in the HQL, and the HQS partner is not present.

In Ref. [23], the author analyzed the doubly heavy tetraquark by using the quark model and found two bound states of T_{bb} with $0(1^+)$. One is the deeply bound state, and the other is the shallow one. The author considered the difference in the two internal structures: The deeply bound state has a very compact structure, while the shallow one is a molecular state. When the author changed the bottom quark to charm or strange quark for the deeply bound state, this binding energy decreased in order of the reduced masses of the diquarks. This behavior was explained by the color electric force which provides attraction for the color $\bar{\mathbf{3}}$ QQ diquark. This color structure indicates that the deeply bound state in Ref. [23] has the spin structure $S_Q = 1, S_q = 0$ because of the Fermi-Dirac statistics. However, in our analysis, T_{cc} and T_{bb} with $0(1^+)$ having the spin structures $S_Q = 0, S_q = 1$ are obtained as the ground state, which means these states contain the color $\mathbf{6}$ QQ diquark.

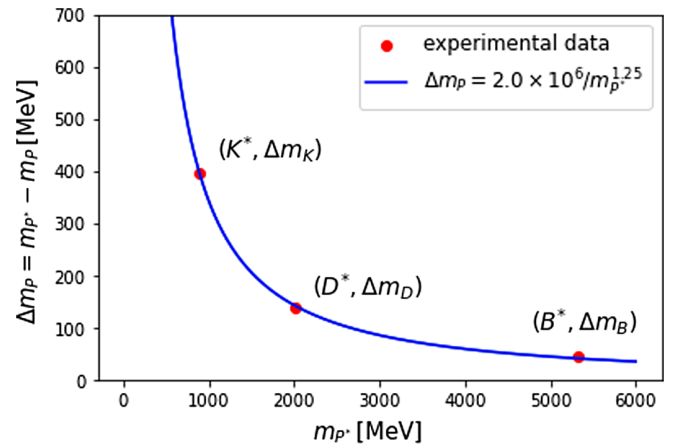


FIG. 9. Heavy vector meson mass dependence of $\Delta m_P = m_{P^*} - m_P$. The dots are the experimental data of K^* , D^* , and B^* from left to right. The solid line is a refitting result referring to Ref. [48], and this result is $\Delta m_P = 2.00 \times 10^6 / m_{P^*}^{1.25}$.

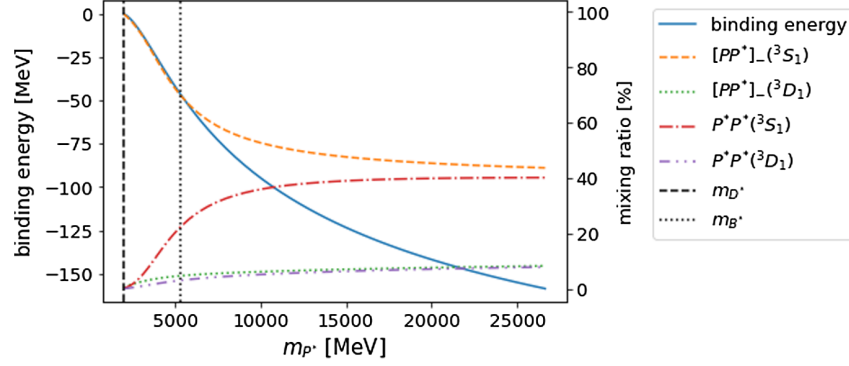


FIG. 10. The mass dependence of the binding energy and mixing ratios of T_{QQ} with $0(1^+)$ for the ground state. The horizontal axis shows the mass of P^* . The vertical dashed and dotted lines indicate $m_{P^*} = m_{D^*}$ and $m_{P^*} = m_{B^*}$, respectively.

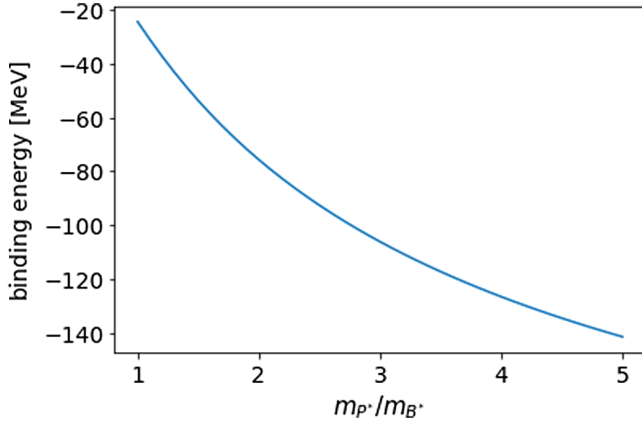


FIG. 11. The mass dependence of the binding energy of T_{QQ} with $0(0^-)$ for the ground state. The horizontal axis shows the ratio between the mass of the heavy vector meson P^* and that of B^* .

The color electric force does not provide an attraction in the color $\mathbf{6}$ QQ diquark, while the tensor force of the meson exchange does. As mentioned in Secs. III A 1 and III B 1, the tensor force of the OPEP is important. The strong tensor force prefers the spin structures $S_Q = 0$, $S_q = 1$ as the origins of T_{cc} and T_{bb} with $0(1^+)$.

For T_{QQ} with $0(0^-)$ and $0(1^-)$ in the HQL, Tables IX and X show that every bound state of T_{QQ} with $0(0^-)$ is degenerate with a certain bound state of T_{QQ} with $0(1^-)$ because of the HQS. As an example, the ground state of T_{QQ} with $0(0^-)$ is degenerate with that of $0(1^-)$. In fact, $V_{\text{boson},0(0^-)}^{\text{LC}}$ and $V_{\text{boson},0(1^-)}^{\text{LC}}$ have the same component, and, hence, these bound states belong to the same HQS multiplet. Figure 11 shows that the T_{bb} bound state for $0(0^-)$ continuously connects to the ground state of T_{QQ} in the HQL, having the spin structure $(S_Q, S_q, J_l) = (1, 1, 1)$. Thus, the origin of the $T_{bb}(0(0^-))$ bound state should belong to the HQS triplet, where $0(1^-)$ and $0(2^-)$ states are present to be the HQS partners. However, in our analysis, no bound state for these quantum numbers is found even for the bottom quark mass region. We expect that these states are found as a resonance above the thresholds. The resonances with $0(1^-)$ and $0(2^-)$ have been discussed in the literature [16,24].

We also study the T_{QQ} states for the isotriplet channel. For $1(0^+)$ and $1(1^+)$ states, Tables XI and XII show that every bound state of T_{QQ} with $1(1^+)$ is degenerate with a certain bound state of T_{QQ} with $1(0^+)$. For the ground states in the HQL, their spin structures are $(S_Q, S_q, J_l) = (0, 0, 0)$ for $1(0^+)$ and $(S_Q, S_q, J_l) = (1, 1, 1)$ for $1(1^+)$.

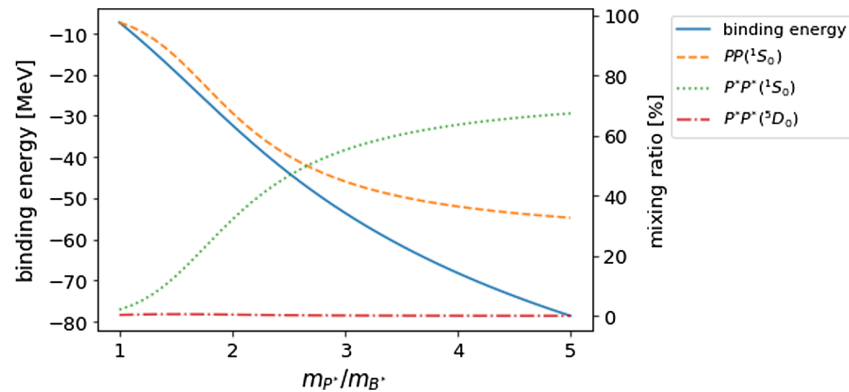


FIG. 12. The mass dependence of the binding energy of T_{QQ} with $1(0^+)$ for the ground state. The same convention as Fig. 11 is used.

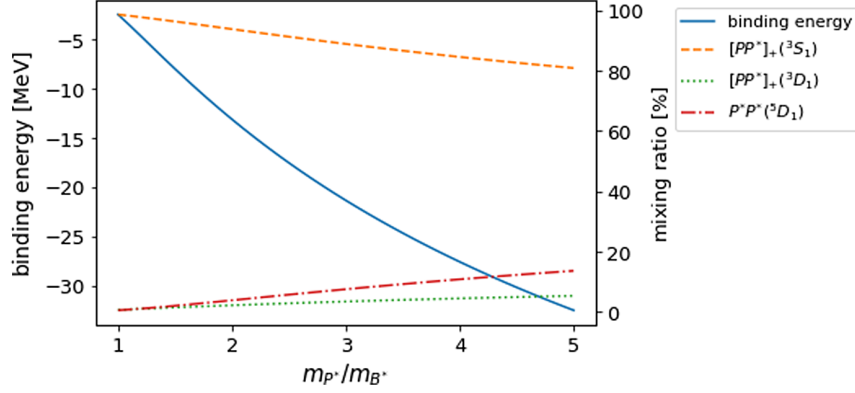


FIG. 13. The mass dependence of the binding energy and mixing ratios of T_{QQ} with $1(1^+)$ for the ground state. The same convention as Fig. 11 is used.

These spin structures indicate that the $1(0^+)$ and $1(1^+)$ ground states belong to the HQS singlet and triplet, respectively. However, the $T_{QQ}(1(1^+))$ ground state is degenerate with the first excited state of $T_{QQ}(1(0^+))$ as shown in Tables XI and XII. Figures 12 and 13 show that the T_{QQ} ground states continuously connect to the T_{bb} bound states. In Table VI, the binding energies of $T_{bb}(1(0^+))$ and $T_{bb}(1(1^+))$ are similar. However, as found in the T_{QQ} , the origins of these T_{bb} bound states in the HQL are different.

Finally, we study the $1(0^-)$ and $1(1^-)$ states. We could not find a bound state for T_{cc} and T_{bb} , while some bound states are obtained in the HQL. Tables XIII and XIV show that every bound state of T_{QQ} with $1(1^-)$ is degenerate with a certain bound state of T_{QQ} with $1(0^-)$. The ground states have the same spin structure $(S_Q, S_q, J_l) = (1, 0, 1)$, indicating that $T_{QQ}(1(0^-))$ and $T_{QQ}(1(1^-))$ are in the same HQS triplet. The remaining state should exist in $1(2^-)$.

IV. SUMMARY

In this paper, we analyzed the doubly heavy tetraquarks as a hadronic molecule of two open-heavy mesons. In the HQL, the heavy pseudoscalar and the heavy vector mesons are degenerate because of the HQS. Thus, we took into account possible $P^{(*)}P^{(*)}$ channel couplings.

As for T_{cc} which has been reported by LHCb in 2022, we considered one-meson exchange force where the cutoff parameter Λ is determined to reproduce the experimental value of the T_{cc} binding energy for $I(J^P) = 0(1^+)$. However, in the case of the OPEP model, we were not able to find a bound state with the reasonable cutoff Λ . By adding the ρ , ω , and σ exchanges (OBEP), we were able to obtain $\Lambda = 1069.8$ MeV, which reproduces the experimental value of T_{cc} . We also calculated the bound-state properties, the wave functions, mixing ratios, and $\sqrt{\langle r^2 \rangle}$, and it can be seen that the channel $[DD^*]_-(^3S_1)$ is a dominant one. Next, we discussed g_s dependence of the binding energy, because the coupling constant g_s for the σ

meson is uncertain. We obtained that this dependence is large. However, by tuning the value of Λ within a reasonable range, we found the set of (g_s, Λ) which reproduces the experimental binding energy of T_{cc} . Also, we studied bound states of T_{cc} with given $I(J^P)$ other than $0(1^+)$. However, we found no bound states of T_{cc} except for $0(1^+)$.

As for T_{bb} in the bottom sector, the T_{bb} bound state with $0(1^+)$ was found for $\Lambda \geq 1010$ MeV even in the OPEP model. This enables us to expect that the T_{bb} bound state with $0(1^+)$ is likely to exist. Also using the OBEP, we calculated the binding energy of T_{bb} with $0(1^+)$ for $\Lambda = 1069.8$ MeV, which reproduces the experimental value of T_{cc} . The binding energy of T_{bb} is 46.0 MeV, and we also obtained the wave functions, mixing ratios, and $\sqrt{\langle r^2 \rangle}$. Then, we found the $[BB^*]_-(^3S_1)$ channel is dominant, and, in addition, the $B^*B^*(^3S_1)$ one is also important unlike T_{cc} . This reason can be understood because the mass difference of B and B^* is smaller than that of D and D^* . This small mass difference leads to the deeply bound state in T_{bb} . Next, we calculated the bound states of T_{bb} with given $I(J^P)$ other than $0(1^+)$ and got bound states. g_s dependence of these bound states is different between $I = 0$ and $I = 1$. As g_s increases, the binding energy decreases for $I = 0$, but the binding energy increases for $I = 1$. This difference is caused by the isospin factor $\vec{\tau}_1 \cdot \vec{\tau}_2$. For $I = 0$, the π and ρ exchange potentials contribute significantly in addition to the σ exchange potential. Therefore, as g_s increases, i.e., Λ decreases, the binding energy becomes smaller. On the other hand, for $I = 1$, since the σ exchange potential is dominant, the binding energy is larger as g_s increases. This enables us to study the σ exchange potential in detail by searching T_{bb} for $I = 1$.

Finally, we considered the spin multiplets of the bound states in the HQL. We have reviewed the light-cloud basis and applied it to T_{cc} with given $I(J^P)$. In the HQL, we obtained many bound states for each quantum number and were able to find that some pairs with different J were degenerate. In this analysis, we found that in the HQL the origin of T_{cc} with $0(1^+)$, which is reported by the LHCb,

had the spin structure $S_Q = 0$, $S_q = 1$. Thus, this state belongs to the HQS singlet, which has no HQS partner in the HQL. We were also able to see that the origin of the bound states of T_{bb} with $0(0^-)$, $1(0^+)$, and $1(1^+)$ have the spin structures $(S_Q, S_q, J_l) = (1, 1, 1)$, $(0, 0, 0)$, and $(1, 1, 1)$, respectively. In the HQL, every bound state of T_{QQ} with $0(0^-)$ is degenerate with a certain bound state of T_{QQ} with $0(1^-)$. In the bottom sector, however, the bound state of T_{bb} with $0(1^-)$ does not exist in our study, while the resonant state may exist. In the isovector channels, we obtained the T_{bb} bound states with $1(0^+)$ and $1(1^+)$. The spin structure in the HQL showed that the origins of these bound states in the HQL were different. In fact, the state of T_{bb} with $1(0^+)$ is a singlet state, while the state of T_{bb} with $1(1^+)$ is a triplet state. Therefore, the resonant states of T_{bb} with $1(0^+)$ and $1(2^+)$ which are partners of $1(1^+)$ may exist.

We have considered only the bound states in this study. As future works, we will investigate the resonant states of T_{cc} and T_{bb} and check the predictions noted

above. We expect to find the bound states and the resonant states of the $P^{(*)}P^{(*)}$ hadronic molecules in future experiments.

As shown in Table V, the obtained size of the T_{bb} bound state is small, $\sqrt{\langle r^2 \rangle} = 0.620$ fm. Thus, the pure hadronic molecular picture would not be suitable to describe such a deeply bound state with the small size. The quark dynamics as discussed by the quark model, etc., would become more important in comparison with the case of T_{cc} . We remain further studies including the quark dynamics in the framework as a future work.

ACKNOWLEDGMENTS

This work is in part supported by Grants-in-Aid for Scientific Research under Grant No. JP20K14478 (Y. Y.).

APPENDIX A: HAMILTONIAN MATRIX

In this section, we show the kinetic and potential matrices for given $I(J^P)$ in the hadronic-molecule basis [16].

1. Kinetic energy matrix

The kinetic energy matrices for given $I(J^P)$ are

$$\begin{aligned}
 K_{0(0^-)} &= \text{diag} \left(-\frac{1}{2\mu_{PP^*}} \Delta_1 \right), \\
 K_{0(1^+)} &= \text{diag} \left(-\frac{1}{2\mu_{PP^*}} \Delta_0, -\frac{1}{2\mu_{PP^*}} \Delta_2, -\frac{1}{2\mu_{P^*P^*}} \Delta_0 + \Delta m_{PP^*}, -\frac{1}{2\mu_{P^*P^*}} \Delta_2 + \Delta m_{PP^*} \right), \\
 K_{0(1^-)} &= \text{diag} \left(-\frac{1}{2\mu_{PP}} \Delta_1, -\frac{1}{2\mu_{PP^*}} \Delta_1 + \Delta m_{PP^*}, -\frac{1}{2\mu_{P^*P^*}} \Delta_1 + 2\Delta m_{PP^*}, \right. \\
 &\quad \left. -\frac{1}{2\mu_{P^*P^*}} \Delta_1 + 2m_{PP^*}, -\frac{1}{2\mu_{P^*P^*}} \Delta_3 + 2m_{PP^*} \right), \\
 K_{1(0^+)} &= \text{diag} \left(-\frac{1}{2\mu_{PP}} \Delta_0, -\frac{1}{2\mu_{P^*P^*}} \Delta_0 + 2\Delta m_{PP^*}, -\frac{1}{2\mu_{P^*P^*}} \Delta_2 + 2\Delta m_{PP^*} \right), \\
 K_{1(0^-)} &= \text{diag} \left(-\frac{1}{2\mu_{PP^*}} \Delta_1, -\frac{1}{2\mu_{P^*P^*}} \Delta_1 + \Delta m_{PP^*} \right), \\
 K_{1(1^+)} &= \text{diag} \left(-\frac{1}{2\mu_{PP^*}} \Delta_0, -\frac{1}{2\mu_{PP^*}} \Delta_2, -\frac{1}{2\mu_{P^*P^*}} \Delta_2 + \Delta m_{PP^*} \right), \\
 K_{1(1^-)} &= \text{diag} \left(-\frac{1}{2\mu_{PP^*}} \Delta_1, -\frac{1}{2\mu_{P^*P^*}} \Delta_1 + \Delta m_{PP^*} \right),
 \end{aligned}$$

where

$$\mu_{P^{(*)}P^{(*)}} = \frac{m_{P^{(*)}} m_{P^{(*)}}}{m_{P^{(*)}} + m_{P^{(*)}}}, \quad \Delta_l = \frac{d^2}{dr^2} - \frac{l(l+1)}{r^2}, \quad \Delta m_{PP^*} = m_{P^*} - m_P.$$

2. Potential matrix in the hadronic-molecule basis

The potential matrices in the hadronic-molecule basis are shown as follows.

(i) $0(1^+)$:

$$\begin{aligned}
V_{\pi,0(1^+)}^{\text{HM}} &= \begin{pmatrix} -C_\pi & \sqrt{2}T_\pi & 2C_\pi & \sqrt{2}T_\pi \\ \sqrt{2}T_\pi & -C_\pi - T_\pi & \sqrt{2}T_\pi & 2C_\pi - T_\pi \\ 2C_\pi & \sqrt{2}T_\pi & -C_\pi & \sqrt{2}T_\pi \\ \sqrt{2}T_\pi & 2C_\pi - T_\pi & \sqrt{2}T_\pi & -C_\pi - T_\pi \end{pmatrix}, \\
V_{v,0(1^+)}^{\text{HM}} &= \begin{pmatrix} C'_v - 2C_v & -\sqrt{2}T_v & 4C_v & -\sqrt{2}T_v \\ -\sqrt{2}T_v & C'_v - 2C_v + T_v & -\sqrt{2}T_v & 4C_v + T_v \\ 4C_v & -\sqrt{2}T_v & C'_v - 2C_v & -\sqrt{2}T_v \\ -\sqrt{2}T_v & 4C_v + T_v & -\sqrt{2}T_v & C'_v - 2C_v + T_v \end{pmatrix}, \\
V_{\sigma,0(1^+)}^{\text{HM}} &= \begin{pmatrix} C_\sigma & 0 & 0 & 0 \\ 0 & C_\sigma & 0 & 0 \\ 0 & 0 & C_\sigma & 0 \\ 0 & 0 & 0 & C_\sigma \end{pmatrix};
\end{aligned}$$

(ii) $0(0^-)$:

$$V_{\pi,0(0^-)}^{\text{HM}} = (C_\pi + 2T_\pi), \quad V_{v,0(0^-)}^{\text{HM}} = (C'_v + 2C_v - 2T_v), \quad V_{\sigma,0(0^-)}^{\text{HM}} = (C_\sigma);$$

(iii) $0(1^-)$:

$$\begin{aligned}
V_{\pi,0(1^-)}^{\text{HM}} &= \begin{pmatrix} 0 & 0 & -\sqrt{3}C_\pi & -2\sqrt{\frac{3}{5}}T_\pi & 3\sqrt{\frac{2}{5}}T_\pi \\ 0 & C_\pi - T_\pi & 0 & -3\sqrt{\frac{3}{5}}T_\pi & -3\sqrt{\frac{2}{5}}T_\pi \\ -\sqrt{3}C_\pi & 0 & -2C_\pi & \frac{2}{\sqrt{5}}T_\pi & -\sqrt{\frac{6}{5}}T_\pi \\ -2\sqrt{\frac{3}{5}}T_\pi & -3\sqrt{\frac{3}{5}}T_\pi & \frac{2}{\sqrt{5}}T_\pi & C_\pi - \frac{7}{5}T_\pi & \frac{\sqrt{6}}{5}T_\pi \\ 3\sqrt{\frac{2}{5}}T_\pi & -3\sqrt{\frac{2}{5}}T_\pi & -\sqrt{\frac{6}{5}}T_\pi & \frac{\sqrt{6}}{5}T_\pi & C_\pi - \frac{8}{5}T_\pi \end{pmatrix}, \\
V_{v,0(1^-)}^{\text{HM}} &= \begin{pmatrix} C'_v & 0 & -2\sqrt{3}C_v & 2\sqrt{\frac{3}{5}}T_v & -3\sqrt{\frac{2}{5}}T_v \\ 0 & C'_v + 2C_v + T_v & 0 & 3\sqrt{\frac{3}{5}}T_v & 3\sqrt{\frac{2}{5}}T_v \\ -2\sqrt{3}C_v & 0 & C'_v - 4C_v & -\frac{2}{\sqrt{5}}T_v & \sqrt{\frac{6}{5}}T_v \\ 2\sqrt{\frac{3}{5}}T_v & 3\sqrt{\frac{3}{5}}T_v & -\frac{2}{\sqrt{5}}T_v & C'_v + 2C_v + \frac{7}{5}T_v & -\frac{\sqrt{6}}{5}T_v \\ -3\sqrt{\frac{2}{5}}T_v & 3\sqrt{\frac{2}{5}}T_v & \sqrt{\frac{6}{5}}T_v & -\frac{\sqrt{6}}{5}T_v & C'_v + 2C_v + \frac{8}{5}T_v \end{pmatrix}, \\
V_{\sigma,0(1^-)}^{\text{HM}} &= \begin{pmatrix} C_\sigma & 0 & 0 & 0 & 0 \\ 0 & C_\sigma & 0 & 0 & 0 \\ 0 & 0 & C_\sigma & 0 & 0 \\ 0 & 0 & 0 & C_\sigma & 0 \\ 0 & 0 & 0 & 0 & C_\sigma \end{pmatrix};
\end{aligned}$$

(iv) $1(0^+)$:

$$\begin{aligned}
V_{\pi,1(0^+)}^{\text{HM}} &= \begin{pmatrix} 0 & -\sqrt{3}C_\pi & \sqrt{6}T_\pi \\ -\sqrt{3}C_\pi & -2C_\pi & -\sqrt{2}T_\pi \\ \sqrt{6}T_\pi & -\sqrt{2}T_\pi & C_\pi - 2T_\pi \end{pmatrix}, \\
V_{v,1(0^+)}^{\text{HM}} &= \begin{pmatrix} C'_v & -2\sqrt{3}C_v & -\sqrt{6}T_v \\ -2\sqrt{3}C_v & C'_v - 4C_v & \sqrt{2}T_v \\ -\sqrt{6}T_v & \sqrt{2}T_v & C'_v + 2C_v + 2T_v \end{pmatrix}, \\
V_{\sigma,1(0^+)}^{\text{HM}} &= \begin{pmatrix} C_\sigma & 0 & 0 \\ 0 & C_\sigma & 0 \\ 0 & 0 & C_\sigma \end{pmatrix};
\end{aligned}$$

(v) $1(0^-)$:

$$\begin{aligned}
V_{\pi,1(0^-)}^{\text{HM}} &= \begin{pmatrix} -C_\pi - 2T_\pi & 2C_\pi - 2T_\pi \\ 2C_\pi - 2T_\pi & -C_\pi - 2T_\pi \end{pmatrix}, \\
V_{\pi,1(0^-)}^{\text{HM}} &= \begin{pmatrix} C'_v - 2C_v + 2T_v & 4C_v + 2T_v \\ 4C_v + 2T_v & C'_v - 2C_v + 2T_v \end{pmatrix}, \\
V_{\sigma,1(0^-)}^{\text{HM}} &= \begin{pmatrix} C_\sigma & 0 \\ 0 & C_\sigma \end{pmatrix};
\end{aligned}$$

(vi) $1(1^+)$:

$$\begin{aligned}
V_{\pi,1(1^+)}^{\text{HM}} &= \begin{pmatrix} C_\pi & -\sqrt{2}T_\pi & -\sqrt{6}T_\pi \\ -\sqrt{2}T_\pi & C_\pi + T_\pi & -\sqrt{3}T_\pi \\ -\sqrt{6}T_\pi & -\sqrt{3}T_\pi & C_\pi - T_\pi \end{pmatrix}, \\
V_{v,1(1^+)}^{\text{HM}} &= \begin{pmatrix} C'_v + 2C_v & \sqrt{2}T_v & \sqrt{6}T_v \\ \sqrt{2}T_v & C'_v + 2C_v - T_v & \sqrt{3}T_v \\ \sqrt{6}T_v & \sqrt{3}T_v & C'_v + 2C_v + T_v \end{pmatrix}, \\
V_{\sigma,1(1^+)}^{\text{HM}} &= \begin{pmatrix} C_\sigma & 0 & 0 \\ 0 & C_\sigma & 0 \\ 0 & 0 & C_\sigma \end{pmatrix};
\end{aligned}$$

(vii) $1(1^-)$:

$$\begin{aligned}
V_{\pi,1(1^-)}^{\text{HM}} &= \begin{pmatrix} -C_\pi + T_\pi & 2C_\pi + T_\pi \\ 2C_\pi + T_\pi & -C_\pi + T_\pi \end{pmatrix}, \\
V_{\pi,1(1^-)}^{\text{HM}} &= \begin{pmatrix} C'_v - 2C_v - T_v & 4C_v - T_v \\ 4C_v - T_v & C'_v - 2C_v - T_v \end{pmatrix}, \\
V_{\sigma,1(1^-)}^{\text{HM}} &= \begin{pmatrix} C_\sigma & 0 \\ 0 & C_\sigma \end{pmatrix},
\end{aligned}$$

$$C_\pi = \frac{1}{3} \left(\frac{g}{2f_\pi} \right)^2 C(r; m_\pi) \vec{\tau}_1 \cdot \vec{\tau}_2, \quad T_\pi = \frac{1}{3} \left(\frac{g}{2f_\pi} \right)^2 T(r; m_\pi) \vec{\tau}_1 \cdot \vec{\tau}_2, \quad C'_v = \left(\frac{\beta g_V}{2m_v} \right)^2 C(r; m_v) \vec{\tau}_1 \cdot \vec{\tau}_2,$$

$$C_v = \frac{1}{3} (\lambda g_V)^2 C(r; m_v) \vec{\tau}_1 \cdot \vec{\tau}_2, \quad T_v = \frac{1}{3} (\lambda g_V)^2 T(r; m_v) \vec{\tau}_1 \cdot \vec{\tau}_2, \quad C_\sigma = - \left(\frac{g_s}{m_\sigma} \right)^2 C(r; m_\sigma).$$

APPENDIX B: LIGHT-CLOUD BASIS

The possible channels, the light-cloud bases, and the potential matrices in the light-cloud basis are shown as follows.
(i) $0(1^+)$:

$$\psi_{0(1^+)}^{\text{HM}} = \begin{pmatrix} |[PP^*]_-(^3S_1)\rangle \\ |[PP^*]_-(^3D_1)\rangle \\ |P^*P^*(^3S_1)\rangle \\ |P^*P^*(^3D_1)\rangle \end{pmatrix},$$

$$\psi_{0(1^+)}^{\text{LC}} = U_{0(1^+)}^{-1} \psi_{0(1^+)}^{\text{HM}} = \begin{pmatrix} |[QQ]_1[S[\bar{q}\bar{q}]_{00}]_1\rangle \\ |[QQ]_0[S[\bar{q}\bar{q}]_{11}]_1\rangle \\ |[QQ]_0[D[\bar{q}\bar{q}]_{11}]_1\rangle \\ |[QQ]_1[D[\bar{q}\bar{q}]_{02}]_1\rangle \end{pmatrix},$$

$$U_{0(1^+)} = \begin{pmatrix} -\frac{1}{\sqrt{2}} & \frac{1}{\sqrt{2}} & 0 & 0 \\ 0 & 0 & \frac{1}{\sqrt{2}} & -\frac{1}{\sqrt{2}} \\ \frac{1}{\sqrt{2}} & \frac{1}{\sqrt{2}} & 0 & 0 \\ 0 & 0 & \frac{1}{\sqrt{2}} & \frac{1}{\sqrt{2}} \end{pmatrix},$$

$$V_{\pi,0(1^+)}^{\text{LC}} = U_{0(1^+)}^{-1} V_{\pi,0(1^+)}^{\text{HM}} U_{0(1^+)} = \begin{pmatrix} -3C_\pi & 0 & 0 & 0 \\ 0 & C_\pi & 2\sqrt{2}T_\pi & 0 \\ 0 & 2\sqrt{2}T_\pi & C_\pi - 2T_\pi & 0 \\ 0 & 0 & 0 & -3C_\pi \end{pmatrix},$$

$$V_{v,0(1^+)}^{\text{LC}} = U_{0(1^+)}^{-1} V_{v,0(1^+)}^{\text{HM}} U_{0(1^+)} = \begin{pmatrix} C'_v - 6C_v & 0 & 0 & 0 \\ 0 & C'_v + 2C_v & -2\sqrt{2}T_v & 0 \\ 0 & -2\sqrt{2}T_v & C'_v + 2C_v + 2T_v & 0 \\ 0 & 0 & 0 & C'_v - 6C_v \end{pmatrix},$$

$$V_{\sigma,0(1^+)}^{\text{LC}} = U_{0(1^+)}^{-1} V_{\sigma,0(1^+)}^{\text{HM}} U_{0(1^+)} = \begin{pmatrix} C_\sigma & 0 & 0 & 0 \\ 0 & C_\sigma & 0 & 0 \\ 0 & 0 & C_\sigma & 0 \\ 0 & 0 & 0 & C_\sigma \end{pmatrix};$$

(ii) $0(0^-)$:

$$\psi_{0(0^-)}^{\text{HM}} = \left(|[PP^*]_+(^3P_0)\rangle \right), \quad \psi_{0(0^-)}^{\text{LC}} = \left(-|[QQ]_1[P[\bar{q}\bar{q}]_{11}]_0\rangle \right),$$

$$V_{\pi,0(0^-)}^{\text{HM}} = (C_\pi + 2T_\pi), \quad V_{v,0(0^-)}^{\text{HM}} = (C'_v + 2C_v - 2T_v), \quad V_{\sigma,0(0^-)}^{\text{HM}} = C_\sigma;$$

(iii) $0(1^-)$:

$$\psi_{0(1^-)}^{\text{HM}} = \begin{pmatrix} |PP(^1P_1)\rangle \\ |[PP^*]_+(^3P_1)\rangle \\ |P^*P^*(^1P_1)\rangle \\ |P^*P^*(^5P_1)\rangle \\ |P^*P^*(^5F_1)\rangle \end{pmatrix},$$

$$\psi_{0(1^-)}^{\text{LC}} = U_{0(1^-)}^{-1} \psi_{0(1^-)}^{\text{HM}} = \begin{pmatrix} |[Q\bar{Q}]_0[P[\bar{q}\bar{q}]_0]_1\rangle \\ |[Q\bar{Q}]_1[P[\bar{q}\bar{q}]_1]_0\rangle \\ |[Q\bar{Q}]_1[P[\bar{q}\bar{q}]_1]_1\rangle \\ |[Q\bar{Q}]_1[P[\bar{q}\bar{q}]_1]_2\rangle \\ |[Q\bar{Q}]_1[F[\bar{q}\bar{q}]_1]_2\rangle \end{pmatrix},$$

$$U_{0(1^-)} = \begin{pmatrix} \frac{1}{2} & \frac{\sqrt{3}}{6} & \frac{1}{2} & \frac{\sqrt{15}}{6} & 0 \\ 0 & \frac{\sqrt{3}}{3} & \frac{1}{2} & -\frac{\sqrt{15}}{6} & 0 \\ \frac{\sqrt{3}}{2} & -\frac{1}{6} & -\frac{\sqrt{3}}{6} & -\frac{\sqrt{5}}{6} & 0 \\ 0 & \frac{\sqrt{5}}{3} & -\frac{\sqrt{15}}{6} & \frac{1}{6} & 0 \\ 0 & 0 & 0 & 0 & 1 \end{pmatrix},$$

$$V_{\pi,0(1^-)}^{\text{LC}} = \begin{pmatrix} -3C_\pi & 0 & 0 & 0 & 0 \\ 0 & C_\pi - 4T_\pi & 0 & 0 & 0 \\ 0 & 0 & C_\pi + 2T_\pi & 0 & 0 \\ 0 & 0 & 0 & C_\pi - \frac{2}{5}T_\pi & \frac{6\sqrt{6}}{5}T_\pi \\ 0 & 0 & 0 & \frac{6\sqrt{6}}{5}T_\pi & C_\pi - \frac{8}{5}T_\pi \end{pmatrix},$$

$$V_{v,0(1^-)}^{\text{LC}} = \begin{pmatrix} C'_v - 6C_v & 0 & 0 & 0 & 0 \\ 0 & C'_v + 2C_v + 4T_v & 0 & 0 & 0 \\ 0 & 0 & C'_v + 2C_v - 2T_v & 0 & 0 \\ 0 & 0 & 0 & C'_v + 2C_v + \frac{2}{5}T_v & -\frac{6\sqrt{6}}{5}T_v \\ 0 & 0 & 0 & -\frac{6\sqrt{6}}{5}T_v & C'_v + 2C_v + \frac{8}{5}T_v \end{pmatrix},$$

$$V_{\sigma,0(1^-)}^{\text{LC}} = \begin{pmatrix} C_\sigma & 0 & 0 & 0 & 0 \\ 0 & C_\sigma & 0 & 0 & 0 \\ 0 & 0 & C_\sigma & 0 & 0 \\ 0 & 0 & 0 & C_\sigma & 0 \\ 0 & 0 & 0 & 0 & C_\sigma \end{pmatrix};$$

(iv) $1(0^+)$:

$$\begin{aligned} \psi_{1(0^+)}^{\text{HM}} &= \begin{pmatrix} |PP(^1S_0)\rangle \\ |P^*P(^1S_0)\rangle \\ |P^*P(^5D_0)\rangle \end{pmatrix}, \\ \psi_{1(0^+)}^{\text{LC}} &= U_{1(0^+)}^{-1} \psi_{1(0^+)}^{\text{HM}} = \begin{pmatrix} |[Q\bar{Q}]_0[S[\bar{q}\bar{q}]_{00}]_0\rangle \\ |[Q\bar{Q}]_1[S[\bar{q}\bar{q}]_{11}]_0\rangle \\ |[Q\bar{Q}]_1[D[\bar{q}\bar{q}]_{11}]_0\rangle \end{pmatrix}, \\ U_{1(0^+)} &= \begin{pmatrix} \frac{1}{2} & \frac{\sqrt{3}}{2} & 0 \\ \frac{\sqrt{3}}{2} & -\frac{1}{2} & 0 \\ 0 & 0 & 1 \end{pmatrix}, \\ V_{\pi,1(0^+)}^{\text{LC}} &= \left(\begin{array}{c|cc} -3C_\pi & 0 & 0 \\ 0 & C_\pi & 2\sqrt{2}T_\pi \\ 0 & 2\sqrt{2}T_\pi & C_\pi - 2T_\pi \end{array} \right), \\ V_{v,1(0^+)}^{\text{LC}} &= \left(\begin{array}{c|cc} C'_v - 6C_v & 0 & 0 \\ 0 & C'_v + 2C_v & -2\sqrt{2}T_v \\ 0 & -2\sqrt{2}T_v & C'_v + 2C_v + 2T_v \end{array} \right), \\ V_{\sigma,1(0^+)}^{\text{LC}} &= \left(\begin{array}{c|cc} C_\sigma & 0 & 0 \\ 0 & C_\sigma & 0 \\ 0 & 0 & C_\sigma \end{array} \right); \end{aligned}$$

(v) $1(0^-)$:

$$\begin{aligned} \psi_{1(0^-)}^{\text{HM}} &= \begin{pmatrix} |[PP^*]_-(^3P_0)\rangle \\ |P^*P(^3P_0)\rangle \end{pmatrix}, \\ \psi_{1(0^-)}^{\text{LC}} &= U_{1(0^-)}^{-1} \psi_{1(0^-)}^{\text{HM}} = \begin{pmatrix} |[Q\bar{Q}]_0[P[\bar{q}\bar{q}]_{10}]_0\rangle \\ |[Q\bar{Q}]_1[P[\bar{q}\bar{q}]_{01}]_0\rangle \end{pmatrix}, \\ U_{1(0^-)} &= \begin{pmatrix} \frac{1}{\sqrt{2}} & -\frac{1}{\sqrt{2}} \\ \frac{1}{\sqrt{2}} & \frac{1}{\sqrt{2}} \end{pmatrix}, \\ V_{\pi,1(0^-)}^{\text{LC}} &= \left(\begin{array}{c|c} C_\pi - 4T_\pi & 0 \\ 0 & -3C_\pi \end{array} \right), \\ V_{\pi,1(0^-)}^{\text{LC}} &= \left(\begin{array}{c|c} C'_v + 2C_v + 4T_v & 0 \\ 0 & C'_v - 6C_v \end{array} \right), \\ V_{\sigma,1(0^-)}^{\text{LC}} &= \left(\begin{array}{c|c} C_\sigma & 0 \\ 0 & C_\sigma \end{array} \right); \end{aligned}$$

(vi) $1(1^+)$:

$$\begin{aligned} \psi_{1(1^+)}^{\text{HM}} &= \begin{pmatrix} |[PP^*]_+(^3S_1)\rangle \\ |[PP^*]_+(^3D_1)\rangle \\ |P^*P^*(^5D_1)\rangle \end{pmatrix}, \\ \psi_{1(1^+)}^{\text{LC}} &= U_{1(1^+)}^{-1} \psi_{1(0^+)}^{\text{HM}} = \begin{pmatrix} |[QQ]_1[S[\bar{q}\bar{q}]_1]_1\rangle \\ |[QQ]_1[D[\bar{q}\bar{q}]_1]_1\rangle \\ |[QQ]_1[D[\bar{q}\bar{q}]_1]_2\rangle \end{pmatrix}, \\ U_{1(1^+)} &= \begin{pmatrix} 1 & 0 & 0 \\ 0 & -\frac{1}{2} & -\frac{\sqrt{3}}{2} \\ 0 & -\frac{\sqrt{3}}{2} & \frac{1}{2} \end{pmatrix}, \\ V_{\pi,1(1^+)}^{\text{LC}} &= \left(\begin{array}{cc|c} C_\pi & 2\sqrt{2}T_\pi & 0 \\ 2\sqrt{2}T_\pi & C_\pi - 2T_\pi & 0 \\ 0 & 0 & C_\pi + 2T_\pi \end{array} \right), \\ V_{v,1(1^+)}^{\text{LC}} &= \left(\begin{array}{cc|c} C'_v + 2C_v & -2\sqrt{2}T_v & 0 \\ -2\sqrt{2}T_v & C'_v + 2C_v + 2T_v & 0 \\ 0 & 0 & C'_v + 2C_v - 2T_v \end{array} \right), \\ V_{\sigma,1(1^+)}^{\text{LC}} &= \left(\begin{array}{cc|c} C_\sigma & 0 & 0 \\ 0 & C_\sigma & 0 \\ 0 & 0 & C_\sigma \end{array} \right); \end{aligned}$$

(vii) $1(1^-)$:

$$\begin{aligned} \psi_{1(1^-)}^{\text{HM}} &= \begin{pmatrix} |[PP^*]_-(^3P_1)\rangle \\ |P^*P^*(^3P_1)\rangle \end{pmatrix}, \\ \psi_{1(1^-)}^{\text{LC}} &= U_{1(1^-)}^{-1} \psi_{1(1^-)}^{\text{HM}} = \begin{pmatrix} |[QQ]_0[P[\bar{q}\bar{q}]_1]_1\rangle \\ |[QQ]_1[P[\bar{q}\bar{q}]_0]_1\rangle \end{pmatrix}, \\ U_{1(1^-)} &= \begin{pmatrix} \frac{1}{\sqrt{2}} & \frac{1}{\sqrt{2}} \\ \frac{1}{\sqrt{2}} & -\frac{1}{\sqrt{2}} \end{pmatrix}, \\ V_{\pi,1(1^-)}^{\text{LC}} &= \left(\begin{array}{c|c} C_\pi + 2T_\pi & 0 \\ 0 & -3C_\pi \end{array} \right), \\ V_{\pi,1(1^-)}^{\text{LC}} &= \left(\begin{array}{c|c} C'_v + 2C_v - 2T_v & 0 \\ 0 & C'_v - 6C_v \end{array} \right), \\ V_{\sigma,1(1^-)}^{\text{LC}} &= \left(\begin{array}{c|c} C_\sigma & 0 \\ 0 & C_\sigma \end{array} \right). \end{aligned}$$

- [1] M. Gell-Mann, A schematic model of baryons and mesons, *Phys. Lett.* **8**, 214 (1964).
- [2] G. Zweig, An SU(3) model for strong interaction symmetry and its breaking. Version 1, Report No. CERN-TH-401, 1964.
- [3] G. Zweig, An SU(3) model for strong interaction symmetry and its breaking. Version 2, in *Developments in the Quark Theory of Hadrons. Vol. 1. 1964–1978*, edited by D. B. Lichtenberg and S. P. Rosen (1964), pp. 22–101.
- [4] N. Brambilla *et al.*, Heavy quarkonium: Progress, puzzles, and opportunities, *Eur. Phys. J. C* **71**, 1534 (2011).
- [5] S. K. Choi *et al.* (Belle Collaboration), Observation of a narrow charmonium-like state in exclusive $B^\pm \rightarrow K^\pm \pi^+ \pi^- J/\psi$ decays, *Phys. Rev. Lett.* **91**, 262001 (2003).
- [6] R. Aaij *et al.* (LHCb Collaboration), Observation of $J/\psi p$ resonances consistent with pentaquark states in $\Lambda_b^0 \rightarrow J/\psi K^- p$ decays, *Phys. Rev. Lett.* **115**, 072001 (2015).
- [7] R. Aaij *et al.* (LHCb Collaboration), Observation of a narrow pentaquark state, $P_c(4312)^+$, and of two-peak structure of the $P_c(4450)^+$, *Phys. Rev. Lett.* **122**, 222001 (2019).
- [8] R. Aaij *et al.* (LHCb Collaboration), Observation of structure in the J/ψ -pair mass spectrum, *Sci. Bull.* **65**, 1983 (2020).
- [9] R. Aaij *et al.* (LHCb Collaboration), Observation of an exotic narrow doubly charmed tetraquark, *Nat. Phys.* **18**, 751 (2022).
- [10] H.-X. Chen, W. Chen, X. Liu, Y.-R. Liu, and S.-L. Zhu, An updated review of the new hadron states, *Rep. Prog. Phys.* **86**, 026201 (2023).
- [11] R. Aaij *et al.* (LHCb Collaboration), Study of the doubly charmed tetraquark T_{cc}^+ , *Nat. Commun.* **13**, 3351 (2022).
- [12] J. P. Ader, J. M. Richard, and P. Taxil, Do narrow heavy multi - quark states exist?, *Phys. Rev. D* **25**, 2370 (1982).
- [13] J. I. Ballot and J. M. Richard, Four quark states in additive potentials, *Phys. Lett.* **123B**, 449 (1983).
- [14] S. Zouzou, B. Silvestre-Brac, C. Gignoux, and J. M. Richard, Four quark bound states, *Z. Phys. C* **30**, 457 (1986).
- [15] N. A. Tornqvist, From the deuteron to deusons, an analysis of deuteron - like meson meson bound states, *Z. Phys. C* **61**, 525 (1994).
- [16] S. Ohkoda, Y. Yamaguchi, S. Yasui, K. Sudoh, and A. Hosaka, Exotic mesons with double charm and bottom flavor, *Phys. Rev. D* **86**, 034019 (2012).
- [17] N. Li, Z.-F. Sun, X. Liu, and S.-L. Zhu, Coupled-channel analysis of the possible $D^{(*)}D^{(*)}.\bar{B}^{(*)}\bar{B}^{(*)}$ and $D^{(*)}\bar{B}^{(*)}$ molecular states, *Phys. Rev. D* **88**, 114008 (2013).
- [18] J.-B. Cheng, Z.-Y. Lin, and S.-L. Zhu, Double-charm tetraquark under the complex scaling method, *Phys. Rev. D* **106**, 016012 (2022).
- [19] F.-L. Wang and X. Liu, Investigating new type of doubly charmed molecular tetraquarks composed of charmed mesons in the H and T doublets, *Phys. Rev. D* **104**, 094030 (2021).
- [20] F.-L. Wang, R. Chen, and X. Liu, A new group of doubly charmed molecule with T-doublet charmed meson pair, *Phys. Lett. B* **835**, 137502 (2022).
- [21] H. Ren, F. Wu, and R. Zhu, Hadronic molecule interpretation of T_{cc}^+ and its beauty partners, *Adv. High Energy Phys.* **2022**, 9103031 (2022).
- [22] T. Asanuma, Y. Yamaguchi, and M. Harada, Analysis of DD^* and $\bar{D}^{(*)}\Xi_{cc}^{(*)}$ molecule by one boson exchange model based on heavy quark symmetry, [arXiv:2311.04695](https://arxiv.org/abs/2311.04695).
- [23] Q. Meng, E. Hiyama, A. Hosaka, M. Oka, P. Gubler, K. U. Can, T. T. Takahashi, and H. S. Zong, Stable double-heavy tetraquarks: Spectrum and structure, *Phys. Lett. B* **814**, 136095 (2021).
- [24] Q. Meng, M. Harada, E. Hiyama, A. Hosaka, and M. Oka, Doubly heavy tetraquark resonant states, *Phys. Lett. B* **824**, 136800 (2022).
- [25] X. Yan, B. Zhong, and R. Zhu, Doubly charmed tetraquarks in a diquark-antidiquark model, *Int. J. Mod. Phys. A* **33**, 1850096 (2018).
- [26] E. J. Eichten and C. Quigg, Heavy-quark symmetry implies stable heavy tetraquark mesons $Q_i Q_j \bar{q}_k \bar{q}_l$, *Phys. Rev. Lett.* **119**, 202002 (2017).
- [27] J.-B. Cheng, S.-Y. Li, Y.-R. Liu, Z.-G. Si, and T. Yao, Double-heavy tetraquark states with heavy diquark-antiquark symmetry, *Chin. Phys. C* **45**, 043102 (2021).
- [28] O. Andreev, $QQ\bar{q}\bar{q}$ potential in string models, *Phys. Rev. D* **105**, 086025 (2022).
- [29] F. S. Navarra, M. Nielsen, and S. H. Lee, QCD sum rules study of QQ - anti-u anti-d mesons, *Phys. Lett. B* **649**, 166 (2007).
- [30] M.-L. Du, W. Chen, X.-L. Chen, and S.-L. Zhu, Exotic $QQ\bar{q}\bar{q}$, $QQ\bar{q}\bar{s}$ and $QQ\bar{s}\bar{s}$ states, *Phys. Rev. D* **87**, 014003 (2013).
- [31] S. S. Agaev, K. Azizi, and H. Sundu, Newly observed exotic doubly charmed meson T_{cc}^+ , *Nucl. Phys.* **B975**, 115650 (2022).
- [32] Q. Xin and Z.-G. Wang, Analysis of the doubly-charmed tetraquark molecular states with the QCD sum rules, *Eur. Phys. J. A* **58**, 110 (2022).
- [33] Q. Xin, Z.-G. Wang, and X.-S. Yang, Analysis of the $X(3960)$ and related tetraquark molecular states via the QCD sum rules, *AAPPS Bull.* **32**, 37 (2022).
- [34] Y. Ikeda, B. Charron, S. Aoki, T. Doi, T. Hatsuda, T. Inoue, N. Ishii, K. Murano, H. Nemura, and K. Sasaki, Charmed tetraquarks T_{cc} and T_{cs} from dynamical lattice QCD simulations, *Phys. Lett. B* **729**, 85 (2014).
- [35] M. Padmanath and S. Prelovsek, Signature of a doubly charm tetraquark pole in DD^* scattering on the lattice, *Phys. Rev. Lett.* **129**, 032002 (2022).
- [36] Y. Lyu, S. Aoki, T. Doi, T. Hatsuda, Y. Ikeda, and J. Meng, Doubly charmed tetraquark T_{cc}^+ from lattice QCD near physical point, *Phys. Rev. Lett.* **131**, 161901 (2023).
- [37] M. Neubert, Heavy quark symmetry, *Phys. Rep.* **245**, 259 (1994).
- [38] B. Grinstein, An Introduction to heavy mesons, in *6th Mexican School of Particles and Fields* (1995), pp. 122–184; [arXiv:hep-ph/9508227](https://arxiv.org/abs/hep-ph/9508227).
- [39] R. Casalbuoni, A. Deandrea, N. Di Bartolomeo, R. Gatto, F. Feruglio, and G. Nardulli, Phenomenology of heavy meson chiral Lagrangians, *Phys. Rep.* **281**, 145 (1997).
- [40] S. Yasui, K. Sudoh, Y. Yamaguchi, S. Ohkoda, A. Hosaka, and T. Hyodo, Spin degeneracy in multi-hadron systems with a heavy quark, *Phys. Lett. B* **727**, 185 (2013).

- [41] Y. Yamaguchi, S. Ohkoda, A. Hosaka, T. Hyodo, and S. Yasui, Heavy quark symmetry in multihadron systems, *Phys. Rev. D* **91**, 034034 (2015).
- [42] Y. Shimizu, Y. Yamaguchi, and M. Harada, Heavy quark spin multiplet structure of $P_c(4312)$, $P_c(4440)$, and $P_c(4457)$, arXiv:1904.00587.
- [43] Y. Yamaguchi, A. Hosaka, S. Takeuchi, and M. Takizawa, Heavy hadronic molecules with pion exchange and quark core couplings: A guide for practitioners, *J. Phys. G* **47**, 053001 (2020).
- [44] S. Ahmed *et al.* (CLEO Collaboration), First measurement of $\Gamma(D^{*+})$. *Phys. Rev. Lett.* **87**, 251801 (2001).
- [45] R. L. Workman *et al.* (Particle Data Group), Review of particle physics, *Prog. Theor. Exp. Phys.* **2022**, 083C01 (2022).
- [46] M.-Z. Liu, T.-W. Wu, M. Pavon Valderrama, J.-J. Xie, and L.-S. Geng, Heavy-quark spin and flavor symmetry partners of the $X(3872)$ revisited: What can we learn from the one boson exchange model?, *Phys. Rev. D* **99**, 094018 (2019).
- [47] C. Isola, M. Ladisa, G. Nardulli, and P. Santorelli, Charming penguins in $B \rightarrow K^* \pi$, $K(\rho, \omega, \phi)$ decays, *Phys. Rev. D* **68**, 114001 (2003).
- [48] Y. Yamaguchi, S. Ohkoda, S. Yasui, and A. Hosaka, Exotic baryons from a heavy meson and a nucleon –negative parity states–, *Phys. Rev. D* **84**, 014032 (2011).